

Cooperative ultrafast nonlinear optical response of molecular nanostructures

Ningjun Wang,^{a)} Vladimir Chernyak,^{b)} and Shaul Mukamel
Center for Photoinduced Charge Transfer, Department of Chemistry, University of Rochester, Rochester, New York 14627

(Received 9 August 1993; accepted 19 October 1993)

The stationary nonlinear reflection and the time resolved four wave mixing signal from a molecular monolayer are calculated using Green function techniques. Cooperative resonant nonlinear response found in small aggregates suggests the existence of coherence size of order of optical wavelength. A new peak in the nonlinear reflection spectrum is predicted, which is missed by the local field approximation. For an infinite two dimensional molecular monolayer with transition dipole moments in the lattice plane, the momentum-dependent two exciton decay rate is found to be larger than the sum of the single exciton radiative decay rates, as predicted by the local field approximation.

I. INTRODUCTION

Studies of optical properties of confined Frenkel excitons in molecular nanostructures are currently drawing considerable interest.¹⁻¹⁴ These follow earlier developments in the investigation of Wannier excitons in semiconductors.¹⁵⁻¹⁷ While the cooperative radiative decay of a single exciton is well studied,¹¹⁻¹³ the radiative decay of exciton pairs is less understood. Pump probe experiments have been commonly used to monitor the one exciton to two exciton transition in semiconductor quantum wells.¹⁸⁻²¹ Such measurements were reported recently in molecular aggregates.^{4,5} Since during the delay period between the pump and the probe the system is in a single exciton state, this technique provides information on single exciton (but not two exciton) dynamics. On the other hand, time resolved four wave mixing (FWM) has been used to study exciton-exciton interactions and two exciton dynamics in semiconductors.²² These experiments are commonly modeled using a simple nonlinear Landau-Ginzburg-Schrödinger equation,^{23,24} which can be derived from the local field approximation (LFA) with some additional assumptions. This theory does not treat the radiative lifetime of two exciton states and does not provide full account for cooperative effects and exciton coherence size.

Recently, Chernyak and Mukamel have derived a Green function expression (GFE) for the third order nonlinear response function of an assembly of two level systems with arbitrary geometry, which properly takes into account retardation and cooperative effects. They treated the electromagnetic field classically, and employed path integral techniques to show how the effects of quantum nature of electromagnetic field may be incorporated.¹² In this paper we apply the GFE to study exciton cooperative effects in a molecular monolayer. We find that for resonant excitation, the nonlinear response function is proportional to the lattice size provided it is much smaller than the

optical wavelength, and is independent of the lattice size when it is much larger than the optical wavelength. We calculate the stationary nonlinear reflection and find a new peak which is missing in the LFA and a simple three level model. We also calculate the time resolved FWM and show how it can be used to study two exciton dynamics. For our geometry, the two exciton decay rate is found to be 1.76 times larger than the sum of single exciton decay rates, while the LFA predicts it to be equal. Conditions for the formation of nonradiative surface excitons are specified.

In Sec. II we summarize the GFE for third order nonlinear response function. In Sec. III we apply the general formulas to a two dimensional monolayer and discuss the nonlinear cooperativity. We calculate and analyze the steady wave nonlinear spectrum in Sec. IV. The time domain FWM signals are calculated and analyzed in Sec. V. Conclusions are given in Sec. VI.

II. REAL SPACE GREEN FUNCTION EXPRESSION FOR FOUR WAVE MIXING

Consider an assembly of two level molecules with arbitrary geometry. We denote the position, the resonance frequency, and the transition dipole moment of molecule m by \mathbf{R}_m , Ω_m , and $\boldsymbol{\mu}_m$. The Hamiltonian is^{11,12}

$$H = \sum_m \Omega_m B_m^+ B_m + \sum_{m \neq n} J_{mn} B_m^+ B_n - \int d^3r \hat{\mathbf{P}}(\mathbf{r}) \cdot \hat{\mathbf{D}}^\perp(\mathbf{r}) + H_{\text{rad}} + 2\pi \int d^3r |\hat{\mathbf{P}}^\perp(\mathbf{r})|^2. \quad (1)$$

B_m^+ and B_m are the exciton creation and annihilation operators for molecule m . They satisfy the commutation relations

$$[B_m, B_n^+] = (1 - 2B_m^+ B_m) \delta_{mn}. \quad (2)$$

J_{mn} is the dipole-dipole interaction between molecules m and n . We will use the point dipole approximation in this paper, therefore

^{a)}Also at University of Rochester, Department of Physics, Rochester, New York 14627.

^{b)}Also at Institute of Spectroscopy, Russian Academy of Sciences, Troitsk, Moscow reg, 142092, Russia.

$$J_{mn} = (1 - \delta_{mn}) \times \frac{R_{mn}^2 (\boldsymbol{\mu}_m \cdot \boldsymbol{\mu}_n)^2 - 3(\mathbf{R}_{mn} \cdot \boldsymbol{\mu}_m)(\mathbf{R}_{mn} \cdot \boldsymbol{\mu}_n)}{R_{mn}^5}, \quad (3)$$

where $\mathbf{R}_{mn} = \mathbf{R}_m - \mathbf{R}_n$. We use the Heitler-London form of the dipole-dipole interaction, which implies that the excitation bandwidth is small compared with the optical frequency. This is an excellent approximation for typical molecular assemblies. The polarization operator is given by

$$\hat{\mathbf{P}}(\mathbf{r}) = \sum_m \hat{\mathbf{P}}_m \delta(\mathbf{r} - \mathbf{R}_m), \quad (4)$$

with

$$\hat{\mathbf{P}}_m = \boldsymbol{\mu}_m (B_m + B_m^\dagger). \quad (5)$$

H_{rad} is the Hamiltonian of radiation field. $\hat{\mathbf{P}}^{\perp}(\mathbf{r})$ and $\hat{\mathbf{D}}^{\perp}(\mathbf{r})$ are the transverse parts of the polarization and electric displacement.^{11,12}

The GFE for the linear polarization in the frequency domain is¹²

$$\mathbf{P}_n^{(1)}(\omega_s) = - \sum_m \hat{\mathbf{R}}_{nm}^{(1)}(\omega_s) \cdot \mathbf{E}_m^{\text{ext}}(\omega_s), \quad (6)$$

where $\mathbf{E}_m^{\text{ext}}$ is the external field, and the linear response function is

$$\hat{\mathbf{R}}_{nm}^{(1)}(\omega_s) = \boldsymbol{\mu}_n \boldsymbol{\mu}_m [\hat{\mathbf{G}}_{nm}(\omega_s) + \hat{\mathbf{G}}_{nm}^*(-\omega_s)]. \quad (7)$$

The $\hat{\mathbf{G}}_{mn}(\omega)$ matrix represents the single particle Green function,^{12,13}

$$\hat{\mathbf{G}}_{mn} = (G(\omega) \cdot \{1 - \phi(\omega) \cdot [G(\omega) + G^*(-\omega)]\}^{-1})_{mn} \quad (8)$$

where $G(\omega)$ is the material Green's function

$$G_{mn}(\omega) = (\omega - H_0 + i\eta)_{mn}^{-1}, \quad (9)$$

and the matrix elements of H_0 are

$$(H_0)_{mn} = \Omega_m \delta_{mn} + J_{mn}. \quad (10)$$

η is a small positive number which is set to $\eta=0$ at the end. In the rotating wave approximation (RWA), Eq. (8) yields

$$\hat{\mathbf{G}}_{mn}(\omega) = [\omega - H^{\text{eff}}(\omega) + i\eta]_{mn}^{-1}, \quad (11)$$

with $H^{\text{eff}}(\omega)$ being the effective Hamiltonian matrix

$$H_{mn}^{\text{eff}}(\omega) = \Omega_m \delta_{mn} + J_{mn} + \phi_{mn}(\omega). \quad (12)$$

$\phi_{mn}(\omega)$ is the material self-energy matrix¹² resulting from the interaction with the transverse electric field. Its real part Δ_{mn} represents a level shift (for $n=m$ this is the Lamb shift and for $n \neq m$ this is the radiative correction to intermolecular interactions). Its imaginary part Γ_{mn} represents radiative decay. The diagonal elements ϕ_{nn} diverge for the point dipole model. Their evaluation thus requires using a more realistic model in which the n th molecule is characterized by a polarization density $\rho_n(\mathbf{r} - \mathbf{R}_n)$ with $\int d^3r \rho(\mathbf{r}) = 1$ [the point dipole limit is recovered when $\rho_n(\mathbf{r} - \mathbf{R}_n) = \delta(\mathbf{r} - \mathbf{R}_n)$]. We then get

$$\phi_{mn}(\omega) \equiv \Delta_{mn}(\omega) - i\Gamma_{mn}(\omega) = \int d\mathbf{r} \int d\mathbf{r}' \rho_m(\mathbf{r} - \mathbf{R}_m) \rho_n(\mathbf{r}' - \mathbf{R}_n) \boldsymbol{\mu}_m \cdot \mathcal{G}^{\perp}(\mathbf{r} - \mathbf{r}', \omega) \cdot \boldsymbol{\mu}_n. \quad (13)$$

\mathcal{G}^{\perp} is the Green function of the transverse electromagnetic field in vacuum

$$\mathcal{G}^{\perp}(\mathbf{r}, \omega) = \int \frac{d^3q}{2\pi^2} \frac{\omega^2}{\omega^2 - q^2 c^2 + i\eta} \left(\mathbf{1} - \frac{\mathbf{q}\mathbf{q}}{q^2} \right) \exp(i\mathbf{q} \cdot \mathbf{r}) = - \left[\left(\frac{\omega}{c} \right)^2 + \nabla \nabla \right] \frac{\exp[i(\omega/c)r]}{r} + \nabla \nabla \frac{1}{r}. \quad (14)$$

It is possible to use the polarization density $\rho_n(\mathbf{r} - \mathbf{R}_n)$ (rather than the point dipole approximation) throughout.¹² In the present calculation, we shall only use it for evaluating the self energy. All other quantities will be evaluated using the point dipole approximation.

For the third order polarization, we have¹²

$$\mathbf{P}_n^{(3)}(\omega_s) = - \frac{1}{8\pi^2} \int d\omega_1 \int d\omega_2 \int d\omega_3 \delta(\omega_s - \omega_1 - \omega_2 - \omega_3) \sum_{m_1, m_2, m_3} \hat{\mathbf{R}}_{nm_1 m_2 m_3}^{(3)}(\omega_s; \omega_1, \omega_2, \omega_3) \mathbf{E}_{m_1}^{\text{ext}}(\omega_1) \mathbf{E}_{m_2}^{\text{ext}}(\omega_2) \mathbf{E}_{m_3}^{\text{ext}}(\omega_3), \quad (15)$$

with the nonlinear response function

$$\begin{aligned} \hat{\mathbf{R}}_{nm_1 m_2 m_3}^{(3)}(\omega_s; \omega_1, \omega_2, \omega_3) = & \sum_{n' n''} \boldsymbol{\mu}_n \boldsymbol{\mu}_{m_1} \boldsymbol{\mu}_{m_2} \boldsymbol{\mu}_{m_3} [\hat{\mathbf{G}}_{nn'}^*(\omega_s) \hat{\mathbf{G}}_{n'm_3}^*(-\omega_3) \hat{\mathbf{G}}_{n''m_2}(\omega_2) \hat{\mathbf{G}}_{n''m_1}(\omega_1) \bar{\Gamma}_{n'n''}(\omega_1 + \omega_2) \\ & + \hat{\mathbf{G}}_{nn'}^*(-\omega_s) \hat{\mathbf{G}}_{n'm_3}(\omega_3) \hat{\mathbf{G}}_{n''m_2}^*(-\omega_2) \hat{\mathbf{G}}_{n''m_1}^*(-\omega_1) \bar{\Gamma}_{n'n''}^*(-\omega_1 - \omega_2)]. \end{aligned} \quad (16)$$

Note that in this equation, the first single particle Green's function is \hat{G}' instead of \hat{G} [Eq. (8)],

$$\hat{G}'_{nn'} = (\{1 - [G(\omega) + G^*(-\omega)] \cdot \phi(\omega)\}^{-1} \cdot G(\omega))_{nn'} \quad (17)$$

where the $G(\omega)$ matrix is given in Eq. (9). Equation (16) generalizes the result of Ref. 12 in which we assumed $\hat{G}' = \hat{G}$, which is justified in the RWA. $\bar{\Gamma}_{n'n''}(\omega_1 + \omega_2)$ is the two exciton scattering matrix²⁵

$$\bar{\Gamma}_{n'n''}(\omega_1 + \omega_2) = -2[F^{-1}(\omega_1 + \omega_2)]_{n'n''}, \quad (18a)$$

$$F_{n'n''}(\omega_1 + \omega_2) = \frac{i}{2\pi} \int d\omega' \hat{G}_{n'n''}(\omega') \hat{G}_{n'n''}(\omega_1 + \omega_2 - \omega'). \quad (18b)$$

Equations (15)–(18) are derived in Ref. 12. We will refer to them as the Green's function expression (GFE).

An alternative way for calculating the nonlinear polarization is by using equations of motion. The Heisenberg equations of motion for the B, B^+ operators are¹²

$$\begin{aligned} \frac{dB_m(t)}{dt} = & -i\Omega_m B_m(t) - i \sum_{n \neq m} J_{mn} [1 - 2B_m^+(t) B_m(t)] \\ & \times B_n(t) + i\mu \cdot \mathbf{E}_m^{\text{ext}}(t) [1 - 2B_m^+(t) B_m(t)] \\ & - \frac{i}{2} \sum_n \int dt' \phi_{mn}(t-t') \\ & \times [B_n(t') + B_n^+(t'), 1 - 2B_m^+(t) B_m(t)]_+, \quad (19) \end{aligned}$$

where $[\cdot]_+$ is an anticommutator. $\phi_{mn}(t-t')$ is the Fourier transform of $\phi_{mn}(\omega)$. The temporal Fourier transform is defined as $F(\omega) = \int dt e^{i\omega t} F(t)$.

The local field approximation (LFA) is equivalent to the factorization approximation²⁵

$$\begin{aligned} \langle B_1^+ \cdots B_m^+ B_{m+1} \cdots B_n \rangle \\ = \langle B_1^+ \rangle \cdots \langle B_m^+ \rangle \langle B_{m+1} \rangle \cdots \langle B_n \rangle. \quad (20) \end{aligned}$$

From Eqs. (19) and (20), we get the LFA result which is the identical to Eq. (16) except that the two exciton scattering matrix should be replaced by

$$\bar{\Gamma}'_{n'n''}(\omega_1 + \omega_2) = -2(\omega_1 + \omega_2 - 2\Omega) \delta_{n'n''}. \quad (21)$$

As will be shown below, the LFA holds only when $\omega_1 + \omega_2$ is tuned off two exciton states.

If we further assume that Ω_m , $\langle B_m(t) \rangle$ and $E_m^{\text{ext}}(t)$ are independent of m , i.e., $\Omega_m = \Omega$, $\langle B_m(t) \rangle = \psi(t)$, $E_m^{\text{ext}}(t) = E(t)$ (uniform excitation of a homogeneous system), and neglect $\phi_{mn}(t-t')$, we obtain the Landau–Ginzburg–Schrödinger equation which has been used in the analysis of four wave mixing in semiconductor nanostructures,²³

$$\begin{aligned} \frac{d\psi}{dt} = & -i[\Omega + J(\mathbf{k}=0)]\psi(t) \\ & + i\mu \cdot \mathbf{E}^{\text{ext}}(t) (1 - 2|\psi(t)|^2) \\ & + 2iJ(\mathbf{k}=0) |\psi(t)|^2 \psi(t). \quad (22) \end{aligned}$$

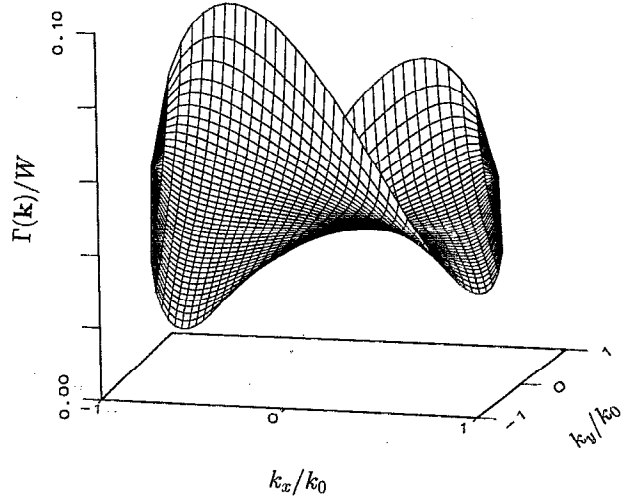


FIG. 1. Momentum dependent single exciton radiative decay rate $\Gamma(k)$ [Eq. (25)]. $W \equiv \mu^2/a^3$.

III. COOPERATIVE EFFECTS IN TWO EXCITON RESONANCES IN MOLECULAR MONOLAYERS

We now apply these results to a two dimensional square molecular lattice with M lattice points. All molecules are assumed to have the same resonance frequency Ω and the same transition dipole moment μ . Translational invariance then implies that J_{mn} , $\phi_{mn}(\omega)$, and $\hat{G}_{mn}(\omega)$ depend on \mathbf{R}_m and \mathbf{R}_n only through $\mathbf{R}_m - \mathbf{R}_n$. We adopt the following convention for spatial Fourier transform:

$$F(\mathbf{k}) = \sum_m F(\mathbf{R}_m) \exp(-i\mathbf{k} \cdot \mathbf{R}_m), \quad (23)$$

with the summation taken over all lattice points.

Hereafter we will use the Markov approximation for the self-energy by setting $\phi(\mathbf{k}, \omega) = \phi(\mathbf{k}, \Omega)$. By doing so we replace the polariton dispersion by exciton dispersion.²⁶ This is usually justified except for $k \simeq \omega/c$. The real part of the material self-energy $\phi(\mathbf{k}, \Omega)$ gives a radiative shift to $J(\mathbf{k})$. For a two dimensional molecular lattice in the dipole approximation for intermolecular interactions, and when $k_0 a \ll 1$ ($k_0 \equiv \Omega/c$), we can neglect the real part of ϕ [which is in order of $(k_0 a)^2 (\mu^2/a^3)$] and obtain (see Appendix A)

$$\phi(\mathbf{k}, \Omega) \simeq -i\Gamma(\mathbf{k}), \quad (24)$$

$$\begin{aligned} \Gamma(\mathbf{k}) = & \frac{2\pi}{a^2} \cdot \frac{k_0^2 \mu^2 - (\mathbf{k} \cdot \boldsymbol{\mu}^{\parallel})^2 - (k_0^2 - k^2) (\mu^{\perp})^2}{\sqrt{k_0^2 - k^2}} \\ & \times \Theta(k_0 - k), \quad (25) \end{aligned}$$

$\Gamma(\mathbf{k})$ is the momentum dependent single exciton radiative decay rate. $\Theta(k_0 - k)$ is the Heaviside step function

$$\Theta(k_0 - k) = \begin{cases} 1 & k < k_0 \\ 0 & k > k_0. \end{cases} \quad (26)$$

Note that $\Gamma(\mathbf{k})$ is always positive. We have denoted the projection of the vector μ parallel and normal to the lattice

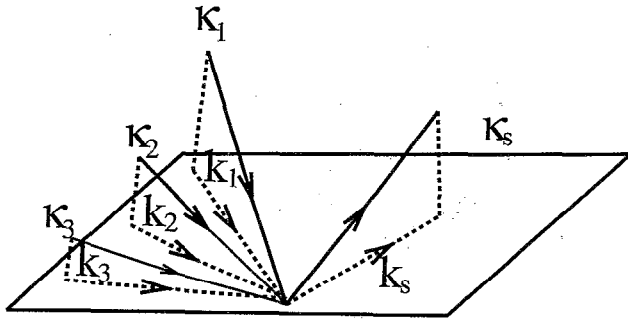


FIG. 2. Configuration of four wave mixing from a molecular monolayer. κ_1, κ_2 , and κ_3 are the incoming wave vectors, and κ_s is the signal. The corresponding projections on the plane are k_1, k_2, k_3 , and k_s .

plane by μ^{\parallel} and μ^{\perp} , respectively. $\Gamma(\mathbf{k})$ as a function of k_x and k_y , for $\mu = (\mu/\sqrt{2})(\hat{x} + \hat{y})$ is displayed in Fig. 1. Here $a\hat{x}$ and $a\hat{y}$ are unit cell vectors.

The external field in a general FWM experiment is [see Fig. (2)]

$$\mathbf{E}_n^{\text{ext}}(\omega) = \sum_{j=1}^3 \mathbf{E}_j^{\text{ext}}(\omega) e^{i\mathbf{k}_j \cdot \mathbf{R}_n} + \sum_{j=1}^3 \mathbf{E}_j^{\text{ext}*}(-\omega) e^{-i\mathbf{k}_j \cdot \mathbf{R}_n}. \quad (27)$$

Substituting Eq. (27) into Eq. (6), we obtain for the linear polarization

$$\mathbf{P}_n^{(1)}(\omega) = \sum_{j=1}^3 \mathbf{P}_{\mathbf{k}_j}(\omega) e^{i\mathbf{k}_j \cdot \mathbf{R}_n} + \sum_{j=1}^3 \mathbf{P}_{\mathbf{k}_j}^*(-\omega) e^{-i\mathbf{k}_j \cdot \mathbf{R}_n}, \quad (28)$$

$$\mathbf{P}_{\mathbf{k}_j}(\omega) = \hat{\chi}^{(1)}(\mathbf{k}_j, \omega) \cdot \mathbf{E}_j^{\text{ext}}(\omega),$$

where

$$\hat{\chi}^{(1)}(\mathbf{k}, \omega) = -\mu\mu [\hat{G}(\mathbf{k}, \omega) + \hat{G}^*(-\mathbf{k}, -\omega)]. \quad (29)$$

Here $G(\mathbf{k}, \omega)$ is the single particle Green function in momentum space

$$\begin{aligned} \hat{R}^{(3)}(-\mathbf{k}_s - \omega_s; -\mathbf{k}_1 - \omega_1, \mathbf{k}_2 \omega_2, \mathbf{k}_3 \omega_3) = & \mu\mu\mu\mu [\hat{G}(\mathbf{k}_s, \omega_s) \hat{G}^*(-\mathbf{k}_3, -\omega_3) \hat{G}(\mathbf{k}_2, \omega_2) \hat{G}(-\mathbf{k}_1, -\omega_1) \bar{\Gamma}(-\mathbf{k}_1 + \mathbf{k}_2, -\omega_1 + \omega_2) \\ & + \hat{G}^*(-\mathbf{k}_s, -\omega_s) \hat{G}(\mathbf{k}_3, \omega_3) \hat{G}^*(-\mathbf{k}_2, -\omega_2) \hat{G}(\mathbf{k}_1, \omega_1) \bar{\Gamma}^*(\mathbf{k}_1 - \mathbf{k}_2, \omega_1 - \omega_2)]. \end{aligned} \quad (35)$$

Note that in momentum space, $\hat{G}'(\mathbf{k}, \omega) = \hat{G}(\mathbf{k}, \omega)$ and we will replace \hat{G}' by \hat{G} everywhere. Here Σ_p denotes summation over all permutations of $-\mathbf{k}_1 - \omega_1, \mathbf{k}_2 \omega_2, \mathbf{k}_3 \omega_3$. Substituting Eqs. (34) and (35) into Eq. (33), the two exciton resonance is contained in

$$\bar{\Gamma}(\mathbf{k}_2 + \mathbf{k}_3, \omega_2 + \omega_3) \equiv -2/F(\mathbf{k}_2 + \mathbf{k}_3, \omega_2 + \omega_3), \quad (36)$$

where

$$F(\mathbf{k}_2 + \mathbf{k}_3, \omega_2 + \omega_3) \equiv \frac{1}{M} \sum_{\mathbf{k}} \frac{1}{\omega_2 + \omega_3 - 2\Omega - J(\mathbf{k}) + i\Gamma(\mathbf{k}) - J(\mathbf{k}_2 + \mathbf{k}_3 - \mathbf{k}) + i\Gamma(\mathbf{k}_2 + \mathbf{k}_3 - \mathbf{k})}. \quad (37)$$

$$\begin{aligned} \hat{G}(\mathbf{k}, \omega) & \equiv \sum_{\mathbf{R}_{mn}} \hat{G}_{mn}(\omega) e^{-i\mathbf{k} \cdot \mathbf{R}_{mn}} \\ & = \frac{1}{\omega - \Omega - J(\mathbf{k}) + i\Gamma(\mathbf{k}) + i\eta}. \end{aligned} \quad (30)$$

The last equality is the result of the RWA, and we denoted the spatial Fourier transforms of J_{mn} and $\bar{\Gamma}_{mn}(\omega)$ by $J(\mathbf{k})$ and $\bar{\Gamma}(\mathbf{k}, \omega)$.

We next calculate the third order nonlinear polarization with wave vector $\mathbf{k}_s \equiv \mathbf{k}_2 + \mathbf{k}_3 - \mathbf{k}_1$. To that end we transform $\hat{R}^{(3)}$ to momentum space

$$\begin{aligned} \hat{R}^{(3)}(-\mathbf{k}_s - \omega_s; -\mathbf{k}_1 - \omega_1, \mathbf{k}_2 \omega_2, \mathbf{k}_3 \omega_3) & = \sum_{m_1 m_2 m_3} \exp[-i\mathbf{k}_1 \cdot (\mathbf{R}_{m_1} - \mathbf{R}_n)] \\ & \times \exp[i\mathbf{k}_2 \cdot (\mathbf{R}_{m_2} - \mathbf{R}_n)] \exp[i\mathbf{k}_3 \cdot (\mathbf{R}_{m_3} - \mathbf{R}_n)] \\ & \times \hat{R}_{nm_1 m_2 m_3}(\omega_s; -\omega_1, \omega_2, \omega_3). \end{aligned} \quad (31)$$

We then get

$$\mathbf{P}_n^{(3)}(\omega_s) = \mathbf{P}_{\mathbf{k}_s}^{(3)}(\omega_s) e^{i\mathbf{k}_s \cdot \mathbf{R}_n} + \dots, \quad (32)$$

$$\begin{aligned} \mathbf{P}_{\mathbf{k}_s}^{(3)}(\omega_s) = & \frac{1}{8\pi^2} \int d\omega_1 \int d\omega_2 \int d\omega_3 \delta(\omega_s + \omega_1 - \omega_2 - \omega_3) \\ & \times \hat{\chi}^{(3)}(-\mathbf{k}_s - \omega_s; -\mathbf{k}_1 - \omega_1, \mathbf{k}_2 \omega_2, \mathbf{k}_3 \omega_3) \\ & \cdot [\mathbf{E}_1^{\text{ext}}(\omega_1)]^* \mathbf{E}_2^{\text{ext}}(\omega_2) \mathbf{E}_3^{\text{ext}}(\omega_3), \end{aligned} \quad (33)$$

where

$$\begin{aligned} \hat{\chi}^{(3)}(-\mathbf{k}_s - \omega_s; -\mathbf{k}_1 - \omega_1, \mathbf{k}_2 \omega_2, \mathbf{k}_3 \omega_3) & = - \sum_p \hat{R}^{(3)}(-\mathbf{k}_s - \omega_s; -\mathbf{k}_1 - \omega_1, \mathbf{k}_2 \omega_2, \mathbf{k}_3 \omega_3), \end{aligned} \quad (34)$$

and

$\bar{\Gamma}$ is responsible for cooperative two exciton effects in $\hat{\chi}^{(3)}$.²⁵ Let us discuss a few limiting cases.

(i) The local field approximation.

In \mathbf{k} space Eq. (21) becomes

$$\bar{\Gamma}^{(L)}(\mathbf{k}_2 + \mathbf{k}_3, \omega_2 + \omega_3) = -2(\omega_2 + \omega_3 - 2\Omega). \quad (38)$$

$\bar{\Gamma}(\mathbf{k}_2 + \mathbf{k}_3, \omega_2 + \omega_3)$ is now independent of M . Therefore, $\hat{\chi}^{(3)}$ is also independent of M , and shows no cooperative effects.

(ii) Off-resonance techniques.

When $\omega_2 + \omega_3$ is detuned far from any two exciton transition, we can neglect all J and Γ in Eq. (36). $\bar{\Gamma}$ then is identical to the LFA [Eq. (38)].

(iii) Resonant excitation of small aggregates

For small aggregates compared with the optical wavelength, the energy splitting of single exciton states ($\sim \mu^2/a^3M$) is much larger than the radiative broadening $\Gamma(\mathbf{k}=0) = M\gamma/2$,¹³ where $\gamma = (4/3)\mu^2(\Omega/c)^3$ is the radiative decay rate of isolated molecule. Let us assume $\omega_2 + \omega_3$ is tuned on resonance with a particular two exciton state so that

$$\omega_2 + \omega_3 \approx 2\Omega + J(\mathbf{k}_0) + J(\mathbf{k}_2 + \mathbf{k}_3 - \mathbf{k}_0),$$

and \mathbf{k}_0 has dominant contribution in the summation of $\Sigma_{\mathbf{k}}$ in Eq. (18). We then get

$$\begin{aligned} \bar{\Gamma}(\mathbf{k}_2 + \mathbf{k}_3, \omega_2 + \omega_3) \\ \approx -2M[\omega_2 + \omega_3 - 2\Omega - J(\mathbf{k}_0) + i\Gamma(\mathbf{k}_0) \\ - J(\mathbf{k}_2 + \mathbf{k}_3 - \mathbf{k}_0) + i\Gamma(\mathbf{k}_2 + \mathbf{k}_3 - \mathbf{k}_0)]. \end{aligned} \quad (39)$$

$\hat{\chi}^{(3)}$ is now proportional to M , which is clear signature of cooperativity.

(iv) Resonant excitation of an infinite monolayer.

When the lattice size is much larger than the optical wavelength λ , the energy splitting of single exciton states [order of $\mu^2/(a^3M)$] is much smaller than the radiative broadening $\Gamma(\mathbf{k})$ [order of $\mu^2/(a^2\lambda)$]. We further tune $\omega_2 + \omega_3$ to be resonant with the two exciton band. The summation in Eq. (36) can then be replaced by an integration

$$\frac{1}{M} \sum_{\mathbf{k}} \rightarrow \frac{a^2}{(2\pi)^2} \int d^2k, \quad (40)$$

$\hat{\chi}^{(3)}$ is independent of M , and cooperativity is lost. This is the natural thermodynamic limit of the present model.

This analysis suggests the existence of a coherence size (order of an optical wavelength) within which molecules have cooperative contributions to $\hat{\chi}^{(3)}$. In the LFA, $\hat{\chi}^{(3)}$ is always independent of M and the cooperativity in case (iii) is completely missed. The LFA therefore breaks down on resonance. Similar arguments were given in Ref. 8 for one dimensional aggregates. The present analysis generalizes these arguments to two dimensional nanostructures. It can also be easily applied to other geometries.

It will be instructive to relate the Green function introduced here to simple properties of the system. The density of single exciton states with momentum \mathbf{k} is

$$\rho_1(\mathbf{k}, \omega) = -\frac{1}{\pi} \text{Im} \hat{G}(\mathbf{k}, \omega). \quad (41)$$

The total single exciton density of states $\bar{\rho}_1(\omega)$ is given by

$$\bar{\rho}_1(\omega) = -\frac{1}{\pi M} \text{Im} \sum_{\mathbf{k}} \hat{G}(\mathbf{k}, \omega). \quad (42)$$

In Appendix B we show that the two exciton density of states with center of mass momentum \mathbf{k} is proportional to the imaginary part of $F(2\mathbf{k}, 2\omega)$

$$\rho_2(\mathbf{k}, \omega) = -\frac{1}{\pi} \text{Im} F(2\mathbf{k}, 2\omega). \quad (43)$$

Note that

$$\bar{\rho}_1(\omega) = 2\rho_2(0, 2\omega) = -\frac{2}{\pi} \text{Im} F(0, 2\omega). \quad (44)$$

The FWM signal generated by the polarization $\mathbf{P}_{\mathbf{k}_s}(t)$ can be obtained by substituting $\mathbf{P}_{\mathbf{k}_s}(t)$ into the Maxwell equations.¹¹ The scattered field at position \mathbf{R} is

$$\begin{aligned} E_{\text{sc}}(\mathbf{R}, t) &= - \sum_n \int \frac{d\omega}{2\pi} e^{-i\omega t} \mathcal{G}^\perp(\mathbf{R} - \mathbf{R}_n, \omega) \cdot \mathbf{P}_n(\omega) \\ &\approx - \sum_n \mathcal{G}^\perp(\mathbf{R} - \mathbf{R}_n, \bar{\omega}_s) \cdot \mathbf{P}_n(t), \end{aligned} \quad (45)$$

where $\bar{\omega}_s \equiv \bar{\omega}_2 + \bar{\omega}_3 - \bar{\omega}_1$ is the central frequency of scattered signal. For R much larger than the wavelength and lattice size (the far field region), we have

$$\mathcal{G}^\perp(\mathbf{R} - \mathbf{R}_n, \omega) \approx -\frac{\omega^2}{Rc^2} (1 - \hat{R}\hat{R}) \exp\left[i\frac{\omega}{c}(\mathbf{R} - \hat{R} \cdot \mathbf{R}_n)\right]. \quad (46)$$

Using Eq. (32) we obtain the signal

$$\begin{aligned} S &= |E_{\text{sc}}(\mathbf{R}, t)|^2 \\ &\approx \frac{M^2 \bar{\omega}_s^4 [(1 - \hat{R}\hat{R}) \cdot \hat{\mu}]^2}{|R|^2 c^4} |P_{\mathbf{k}_s}(t)|^2 \delta_{\mathbf{k}_s, \bar{\omega}_s \hat{R}^\parallel / c}. \end{aligned} \quad (47)$$

Here $\hat{\mu} = \boldsymbol{\mu}/\mu$, and \hat{R}^\parallel is the projection of \mathbf{R}/R in the plane. The signal wave vector is $\hat{\mathbf{k}}_s = (\bar{\omega}_s/c)\hat{R}$ whose projection in the plane is \mathbf{k}_s . Note that the signal is proportional to $|P_{\mathbf{k}_s}(t)|^2$.

IV. STATIONARY NONLINEAR REFLECTION

In a nonlinear reflection experiment, a single beam with wave vector $\boldsymbol{\kappa}$ and frequency ω is incident on the monolayer. The polarization with wave vector \mathbf{k} (the projection of $\boldsymbol{\kappa}$ in the plane) to third order in the external field is

$$\begin{aligned} \mathbf{P}_{\mathbf{k}}(\omega) &= \hat{\chi}^{(1)}(\mathbf{k}, \omega) \cdot \mathbf{E}^{\text{ext}} \\ &+ \hat{\chi}^{(3)}(\mathbf{k}\omega; -\mathbf{k}-\omega, \mathbf{k}\omega, \mathbf{k}\omega) \cdot (\mathbf{E}^{\text{ext}})^* \mathbf{E}^{\text{ext}} \mathbf{E}^{\text{ext}}. \end{aligned} \quad (48)$$

The reflected signal S is (up to a proportionality factor)

$$S(\mathbf{k}, \omega) = |P_{\mathbf{k}}(\omega)|^2 = S_{\text{LR}}(\mathbf{k}, \omega) + S_{\text{NR}}(\mathbf{k}, \omega), \quad (49)$$

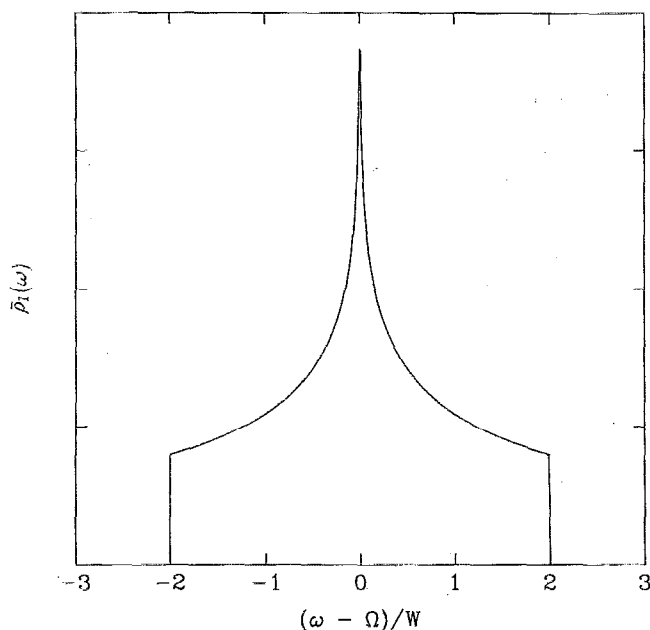


FIG. 3. Single exciton density of states of a two dimensional molecular monolayer calculated using Eq. (42).

where $S_{LR}(\mathbf{k}, \omega)$ and $S_{NR}(\mathbf{k}, \omega)$ are the linear and nonlinear contributions to the reflection signal,

$$S_{LR}(\mathbf{k}, \omega) = |\hat{\chi}^{(1)}(\mathbf{k}, \omega) \cdot \mathbf{E}^{\text{ext}}|^2,$$

$$S_{NR}(\mathbf{k}, \omega) = 2 \text{Re}\{[\hat{\chi}^{(1)}(\mathbf{k}, \omega) \cdot \mathbf{E}^{\text{ext}}]^* \cdot \hat{\chi}^{(3)}(\mathbf{k}\omega; -\mathbf{k} - \omega, \mathbf{k}\omega, \mathbf{k}\omega) \cdot (\mathbf{E}^{\text{ext}})^* \mathbf{E}^{\text{ext}} \mathbf{E}^{\text{ext}}\} + O(E^6).$$
(50)

The nonlinear part corresponds to heterodyne detection of the signal where the linear reflection serves as the local oscillator.²⁷ By substituting Eqs. (29) and (34) into Eq. (50) and invoking the RWA, we find (up to an overall proportionality factor)

$$S_{LR}(\mathbf{k}, \omega) = \mu^4 |\hat{G}(\mathbf{k}, \omega)|^2, \quad (51)$$

$$S_{NR}(\mathbf{k}, \omega) = \mu^6 |\hat{G}(\mathbf{k}, \omega)|^4 \text{Re}[\hat{G}(\mathbf{k}, \omega) \bar{\Gamma}(2\mathbf{k}, 2\omega)]. \quad (52)$$

We have performed numerical calculations for a two dimensional infinite square lattice with unit cell vectors $a\hat{x}$ and $a\hat{y}$, and $k_0 \equiv \Omega/c = 2\pi/(1000a)$. All molecules have the same in-plane transition dipole moment

$$\boldsymbol{\mu} = \frac{\mu}{\sqrt{2}} (\hat{x} + \hat{y}).$$

We further assume nearest neighbor interactions, so that

$$J(\mathbf{k}) = -W[\cos(k_x a) + \cos(k_y a)]. \quad (53)$$

Here \mathbf{k} is the two dimensional in plane momentum vector, and $4W$ is the exciton bandwidth, with

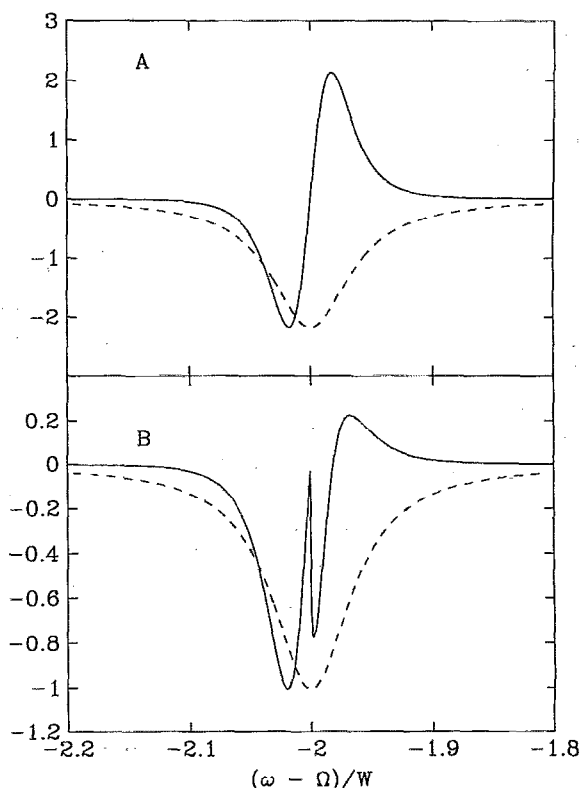


FIG. 4. The frequency dependent linear $S_{LR}(0, \omega)$ (dash) and nonlinear $S_{NR}(0, \omega)$ (solid) reflection signal [see Eq. (50)]. Here we plot the negative linear signal and normalize it to have the same height as the negative peak of the nonlinear signal. (A) is the result of LFA. (B) is the result of GFE formula. The vertical scale shows the relative magnitude of the signal. The nonlinear reflection signal from an anharmonic oscillator Eq. (55) with $\Omega_0 - \Omega = J(k=0) = -2W$, $\gamma = 2\Gamma(k=0)$, $\mu' = 3.99\mu$, and $g/W = 0.001$ coincides with the LFA curve [solid line in (A)].

$$W \equiv \frac{\mu^2}{a^3}. \quad (54)$$

The single exciton density of states $\bar{\rho}_1(\omega)$ [Eq. (42)] for this geometry is displayed in Fig. 3.

Before calculating the signal using the GFE, we consider first the local field approximation, [Eqs. (35) and (38)]. The linear $S_{LR}(0, \omega)$ (dash line) and the nonlinear $S_{NR}(0, \omega)$ (solid line) reflection spectra are shown in panel (A) of Fig. 4. This is a typical spectrum for a three level system shown in Fig. 5(B). The negative peak represents bleaching of the ground state to one exciton state transition. The positive component represents induced reflection caused by the one exciton to two exciton transitions.

The LFA result can be reproduced by the following anharmonic oscillator model:

$$H = \Omega_0 C^+ C + \frac{g}{2} (C^+)^2 C^2. \quad (55)$$

C and C^+ are the Bose operators

$$[C, C^+] = 1, \quad (56)$$

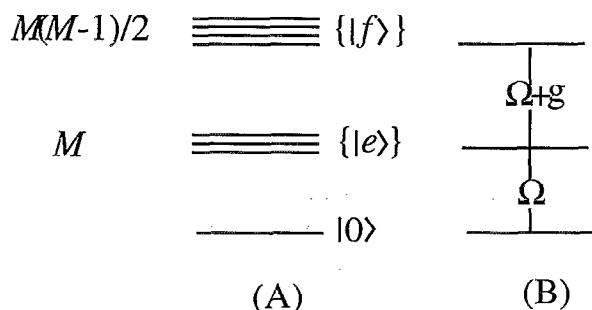


FIG. 5. (A) Energy level scheme of a molecular monolayer. The system has a ground state $|0\rangle$, M single exciton states $|e\rangle$, and $M(M-1)/2$ two exciton states $|f\rangle$. Due to momentum conservation, only one single exciton state, and those two exciton states with center of mass momentum $2k$ need to be considered in a given nonlinear reflection experiment. For impulsive FWM, two single exciton states (with momenta k_1 and k_2), and those two exciton states with center of mass momentum $2k_2$ need to be considered. (B) Level scheme for the anharmonic oscillator model Eq. (55).

and g is a diagonal anharmonicity. The eigenstates that contribute to $\hat{\chi}^{(3)}$ are the ground state (energy 0), the first excited state (energy Ω_0), and the second excited state (energy $2\Omega_0 + g$). The level scheme is shown in Fig. 5(B). The imaginary part of molecular self energy is taken to be $\text{Im } \phi = -i\gamma/2$, and the polarization operator is

$$\hat{P} = \mu(C + C^\dagger). \quad (57)$$

Using the GFE for finite g^{12} and the RWA, we obtain the linear and nonlinear reflection signal (up to a proportionality factor)

$$S_{\text{LR}}(\omega) = |\hat{\chi}^{(1)}(\omega)|^2 = \frac{|\mu'|^4}{|\omega - \Omega_0 + i\gamma/2|^2}, \quad (58)$$

$$S_{\text{NR}}(\omega) = \text{Re}[\hat{\chi}^{(1)*} \hat{\chi}^{(3)}(\omega)] \\ = \frac{4g(2\omega - 2\Omega_0 - g)|\mu'|^6}{|\omega - \Omega_0 + i\gamma/2|^4 \cdot |2\omega - 2\Omega_0 - g + i\gamma|^2}. \quad (59)$$

To compare with the two dimensional monolayer, we chose $\Omega_0 = \Omega + J(k=0)$, $\gamma = 2\Gamma(k=0)$. Taking $\mu' = \mu$, we find that $S_{\text{LR}}(\omega)$ is equal to that of the monolayer. Taking $g/W = 0.001$, the line shape of $S_{\text{NR}}(\omega)$ coincides with that of the monolayer under the LFA [Fig. 4(A) solid line]. However, we have to take $\mu' = 3.99\mu$ to fit the intensity. Fitting the linear and nonlinear signal requires different values of parameter μ' . This shows that although the anharmonic oscillator model can reproduce the linear and the nonlinear reflection spectrum in the LFA, it cannot account for their relative magnitudes.

We next consider the full GFE expression [Eq. (52) together with Eqs. (30), (36), and (37)]. The k summation in Eq. (37) is replaced by an integral [Eq. (40)]. The result [shown in Fig. 4(B)] is qualitatively different from the LFA. There is a new negative peak at the band edge. Obviously the real system has many two exciton states and cannot be represented by a three level model. The system

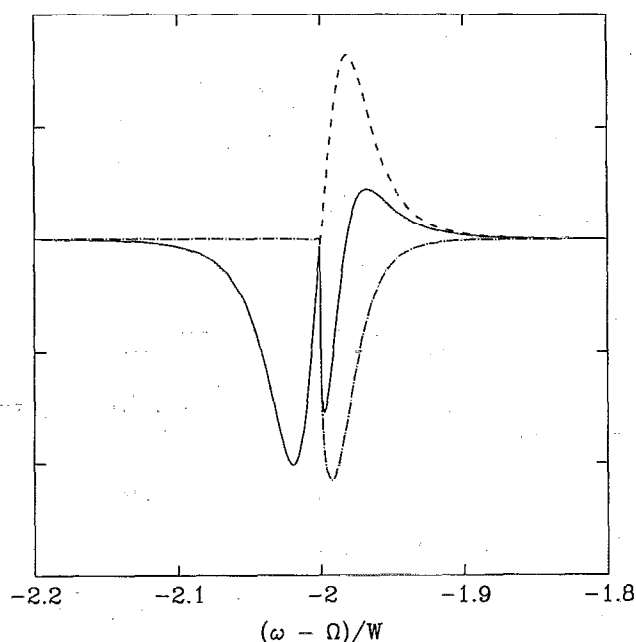


FIG. 6. The two contributions to the nonlinear reflection signal Eq. (60). Shown is the first term (dash), the second term (dash-dot), and their sum (solid).

looks like a collection of M anharmonic oscillators with different damping rates, and cannot be represented by a single oscillator. In order to trace the origin of this additional negative peak, we rewrite Eq. (52) as

$$S_{\text{NR}}(\mathbf{k}, \omega) = -\frac{2\mu^6 |G(\mathbf{k}, \omega)|^4}{|F(2\mathbf{k}, 2\omega)|^2} \cdot \text{Re } G(\mathbf{k}, \omega) \text{Re } F(2\mathbf{k}, 2\omega) \\ - \frac{2\mu^6 |G(\mathbf{k}, \omega)|^4}{|F(2\mathbf{k}, 2\omega)|^2} \cdot \text{Im } G(\mathbf{k}, \omega) \text{Im } F(2\mathbf{k}, 2\omega). \quad (60)$$

Note that the second term is proportional to the product of single exciton density of states with momentum k and two exciton density of states with center of mass momentum $2k$. Choosing $k=0$, we plot in Fig. 6 the first and the second terms in the above equation (dash and dash-dot curves, respectively). Their sum yield $S_{\text{NR}}(\mathbf{k}, \omega)$ and is displayed in solid line. From the figure with see that the additional negative peak is caused by the second term of Eq. (60). Figure 3 shows that $\bar{\rho}_1(\omega) = -(2/\pi) \text{Im } F(0, 2\omega)$ increases sharply when ω approaches the bandedge from the red side. This causes the additional negative peak at the bandedge. Therefore, this additional peak is caused by the sharp edge of two exciton density of states (with center of mass momentum 0) at the bandedge. The sharp edge of two exciton density of states is not a sufficient condition for the appearance of the additional peak. To demonstrate this, we will use a Kramers-Kronig representation for the nonlinear response function²⁸

$$\begin{aligned}
\hat{\chi}^{(3)}(\omega_s; \omega_1, \omega_2, \omega_3) \\
&= \hat{\chi}^{(3)}(\omega_s; \omega_1, \omega_2, \omega_3; \mathbf{k}_s = \mathbf{k}_1 = \mathbf{k}_2 = \mathbf{k}_3 = 0) \\
&= \sum_p \frac{1}{8\pi^3} \int d\epsilon' \int d\epsilon \int d\epsilon'' \kappa(\epsilon', \epsilon, \epsilon'') \\
&\quad \times \left[\frac{1}{\omega_1 - \epsilon' + i\eta} \cdot \frac{1}{\omega_1 + \omega_2 - \epsilon + i\eta} \right. \\
&\quad \left. \times \left(\frac{1}{\omega_s - \epsilon'' + i\eta} + \frac{1}{-\omega_3 - \epsilon'' - i\eta} \right) + c'.c' \right], \quad (61)
\end{aligned}$$

where $c'.c'$ denote sending $\omega_i \rightarrow -\omega_i, i=1,2,3,s$ and then taking complex conjugation, and

$$\begin{aligned}
\kappa(\epsilon', \epsilon, \epsilon'') &\equiv (2\pi)^3 \text{Tr} [P\delta(\epsilon'' - H)P\delta(\epsilon - H) \\
&\quad \times P\delta(\epsilon' - H)P\rho_g]. \quad (62)
\end{aligned}$$

In Appendix C we calculate $\kappa(\epsilon', \epsilon, \epsilon'')$ for our model [Eq. (C15)].

We will now compare the nonlinear reflection signal from the monolayer with the prediction of a simple statistical model which uses the actual one particle and two particle density of states, but assumes that all transition dipole matrix elements are identical, i.e., $\langle e|\hat{P}|0\rangle = \mu$ and $\langle f|\hat{P}|e\rangle = \mu'$ for all single exciton states $\{|e\rangle\}$ and two exciton states $\{|f\rangle\}$. For this simple model we have

$$\kappa(\epsilon', \epsilon, \epsilon'') = \kappa_0(\epsilon', \epsilon, \epsilon'') + \mu^2 \mu'^2 \rho_1(\epsilon') \rho_2(\epsilon) \rho_1(\epsilon''), \quad (63)$$

where $\kappa_0(\epsilon', \epsilon, \epsilon'')$ corresponds to the nonlinear response of a two level system. Substituting $\rho_1(\epsilon)$ and $\rho_2(\epsilon)$ by $-(1/\pi)\text{Im} G(0, \epsilon)$ and $-(1/\pi)\text{Im} F(0, \epsilon)$, using κ from Eq. (63) to Eq. (61), performing the integration over ϵ', ϵ and ϵ'' , and substituting $\hat{\chi}^{(3)}$ from Eq. (61) in Eq. (50), we obtain the statistical nonlinear signal S_{NRS} ,

$$S_{\text{NRS}}(\omega) = S_{\text{NRS}}^{\text{I}}(\omega) + S_{\text{NRS}}^{\text{II}}(\omega), \quad (64a)$$

$$S_{\text{NRS}}^{\text{I}}(\omega) \simeq \frac{\mu^6}{[(\omega - E_0)^2 + \Gamma_0^2]^2}, \quad (64b)$$

$$S_{\text{NRS}}^{\text{II}}(\omega) \simeq \frac{\mu^4 \mu'^2}{[(\omega - E_0)^2 + \Gamma_0^2]^2} (\omega - E_0) \text{Re}[F(0, 2\omega)], \quad (64c)$$

where $E_0 = \Omega + J(\mathbf{k}=0)$ and $\Gamma_0 = \Gamma(\mathbf{k}=0)$. $S_{\text{NRS}}^{\text{I}}$ contains the contribution of single exciton states $\{|e\rangle\}$ while $S_{\text{NRS}}^{\text{II}}$ contains the two exciton contribution $\{|f\rangle\}$. To estimate these terms, we neglect effects of retardation in exciton scattering. Substituting G from Eq. (9) to Eq. (18b) we get in the resonant region

$$\text{Re}[F(0, 2\omega)] \sim (4W)^{-1} \ln \left[\frac{16W^2}{(\omega - E_0)^2} \right], \quad (65)$$

where $4W$ is the bandwidth. For $\mu' \gg \mu$ we have $S_{\text{NRS}}^{\text{II}} \gg S_{\text{NRS}}^{\text{I}}$. Substituting Eq. (65) to Eq. (64), we obtain

$$\begin{aligned}
S_{\text{NRS}} &\simeq \frac{\mu^4 \mu'^2}{[(\omega - E_0)^2 + \Gamma_0^2]^2} (\omega - E_0) \\
&\quad \times (4W)^{-1} \ln \left[\frac{16W^2}{(\omega - E_0)^2} \right]. \quad (66)
\end{aligned}$$

We can see from Eq. (66) that there are two peaks (one negative and the other positive) in the frequency dependence of $S_{\text{NRS}}(\omega)$ [just like Fig. 4(A)] with no additional peak. Therefore, not any system whose two exciton density of states has a sharp edge creates the additional peak in the nonlinear reflection spectrum.

In contrast, if we use $\kappa(\epsilon', \epsilon, \epsilon'')$ for the real monolayer [Eq. (C15)] to evaluate the nonlinear signal we obtain Eq. (60). Denoting the first and the second terms in the right-hand side of Eq. (60) by S_{NR}^{I} and $S_{\text{NR}}^{\text{II}}$, and using Eq. (65), we have

$$S_{\text{NR}}^{\text{I}}(\omega) \simeq \frac{\mu^6}{[(\omega - E_0)^2 + \Gamma_0^2]^3} \cdot \frac{4W(\omega - E_0)}{\ln[(4W)^2/(\omega - E_0)^2]}. \quad (67)$$

Equations (66) and (67) show that although there are two peaks (one positive and the other negative) in the frequency dependence of both S_{NRS} and S_{NR}^{I} , this dependence is quite different. The reason can be seen from Eq. (C15). The matrix elements of the polarization between one and two particle states of the real system are nonzero only for two exciton energy ϵ with $|\epsilon - 2E_0| \sim \Gamma_0$, while for the statistical model they are assumed to be the same for all states. To get the exact frequency dependence of the signal with the additional peak, one should use the exact expression for κ [Eq. (C15)] which gives the term $S_{\text{NR}}^{\text{II}}$ in addition to S_{NR}^{I} in the signal. Note that neglecting effects of retardation in the two exciton scattering matrix which is a good approximation for $|\omega - E_0| \simeq \Gamma_0 \gg |J(k=\omega/c) - J(k=0)|$, does not imply that we neglect radiative decay effects of two exciton states. This can be seen from Eq. (C15): the expression for κ contains besides $F(\epsilon)$ the term

$$\frac{1}{\epsilon - \epsilon' - E_0 + i\Gamma_0} \cdot \frac{1}{\epsilon - \epsilon'' - E_0 + i\Gamma_0},$$

which depends on the two exciton state energy ϵ and contains the radiative damping rate Γ_0 .

V. IMPULSIVE FOUR WAVE MIXING

In this section, we apply the GFE to a time domain FWM experiment.^{22,23} Two laser pulses centered at times $t_1 = -\tau$ and $t_2 = 0$ with frequencies $\bar{\omega}_1, \bar{\omega}_2$ and wave vectors κ_1, κ_2 interact with the sample. The external field is

$$\mathbf{E}_n^{\text{ext}}(t) = \mathbf{E}_1^{\text{ext}}(t + \tau) e^{i\kappa_1 \cdot \mathbf{R}_n} + \mathbf{E}_2^{\text{ext}}(t) e^{i\kappa_2 \cdot \mathbf{R}_n} + \text{c.c.} \quad (68)$$

We consider the signal generated in the direction $\mathbf{k}_s \equiv 2\mathbf{k}_2 - \mathbf{k}_1$. We further assume that both excitation pulses are short compared with the exciton radiative lifetime $1/\Gamma(\mathbf{k})$, we therefore set $\mathbf{k}_2 = \mathbf{k}_3$ and $\mathbf{E}_2^{\text{ext}}(\omega) = \mathbf{E}_3^{\text{ext}}(\omega) \equiv \mathbf{E}_2^{\text{ext}}, \mathbf{E}_1^{\text{ext}}(\omega) = \mathbf{E}_1^{\text{ext}} e^{-i\omega\tau}$ in Eq. (33), then

carry out the ω_2 and ω_3 integrations analytically, and perform the Fourier transform with respect to ω_s , to obtain (up to a proportionality factor)

$$\begin{aligned} P_{\mathbf{k}_s}^{(3)}(t, \tau) &= \frac{1}{2\pi} \exp[-i(\Omega + J_s - i\Gamma_s)(t + \tau)] \Theta(t + \tau) \\ &\times \int d\omega_1 \frac{1 - \exp[-i(\omega_1 - \Omega_s)(t + \tau)]}{\omega_1 - \Omega_s} \\ &\times \frac{\exp(i\omega_1 \tau)}{\omega_1 - 2\Omega - 2J_2 + 2i\Gamma_2} \cdot \bar{\Gamma}(2\mathbf{k}_2, \omega_1), \quad (69) \end{aligned}$$

where $\Omega_s \equiv 2\Omega + J_s - i\Gamma_s + J_1 + i\Gamma_1$. We have used J_i, Γ_i to denote $J(\mathbf{k}_i), \Gamma(\mathbf{k}_i)$, $i=1,2,s$ in the remaining of the paper. For comparison, in the LFA we have

$$\begin{aligned} |P_{\mathbf{k}_s}^{(3)}(t, \tau > 0)|^2 &= 4 \frac{e^{-2\Gamma_1 \tau} e^{-2\Gamma_s t}}{|D|^2} \\ &\times |J_1 + i\Gamma_1 + J_s - i\Gamma_s - 2(J_2 - i\Gamma_2)e^{iD\tau}|^2, \quad (70a) \end{aligned}$$

$$|P_{\mathbf{k}_s}^{(3)}(t, \tau < 0)|^2 = 16e^{-2\Gamma_s t_0} e^{-4\Gamma_2 |\tau|} |J_2 - i\Gamma_2|^2 \cdot \left| \frac{1 - e^{iD\tau}}{D} \right|^2, \quad (70b)$$

where $D = J_1 + i\Gamma_1 - 2J_2 + 2i\Gamma_2 + J_s - i\Gamma_s$, $\Gamma_i = \Gamma(\mathbf{k}_i)$, $i=1,2,s$, and $t_0 = t - |\tau|$.

We performed numerical calculations using the same geometry of Sec. IV. Since $k_2 a \ll 1$, we approximate $\bar{\Gamma}(2\mathbf{k}_2, \omega_1)$ in Eq. (69) by $\bar{\Gamma}(0, \omega_1)$. The time integrated FWM signal is

$$S(\tau) = \int dt |P_{\mathbf{k}_s}^{(3)}(t, \tau)|^2. \quad (71)$$

Equation (69) holds for both positive and negative delay times. Since the accessible eigenstates and the relevant dynamics are very different for negative and for positive delay τ , we will analyze them separately.

First we consider positive delay ($\tau > 0$). Equations (69) and (70) give

$$|P_{\mathbf{k}_s}^{(3)}(t, \tau)|^2 = e^{-2\Gamma_1 \tau} |P_{\mathbf{k}_s}^{(3)}(t, 0)|^2, \quad (72)$$

which yield

$$S(\tau) \sim \exp[-2\Gamma_1 \tau]. \quad (73)$$

Therefore, from the measurement of $S(\tau)$, we obtain the wave vector dependent single exciton radiative decay rate $2\Gamma(\mathbf{k})$.

This result can be understood using Fig. 7(A) which shows that the sample interacts with E_1^{ext} once creating a state $|0\rangle\langle\mathbf{k}_1|$. Here $|\mathbf{k}_1\rangle = B_{\mathbf{k}_1}^+ |0\rangle$ is a single exciton eigenstate with momentum \mathbf{k}_1 . $B_{\mathbf{k}}, B_{\mathbf{k}}^+$ are exciton creation and annihilation operators in momentum space,⁶

$$B_{\mathbf{k}} = \frac{1}{\sqrt{M}} \sum_m B_m e^{-i\mathbf{k} \cdot \mathbf{R}_m}, \quad (74a)$$

$$B_{\mathbf{k}}^+ = \frac{1}{\sqrt{M}} \sum_m B_m^+ e^{i\mathbf{k} \cdot \mathbf{R}_m}. \quad (74b)$$

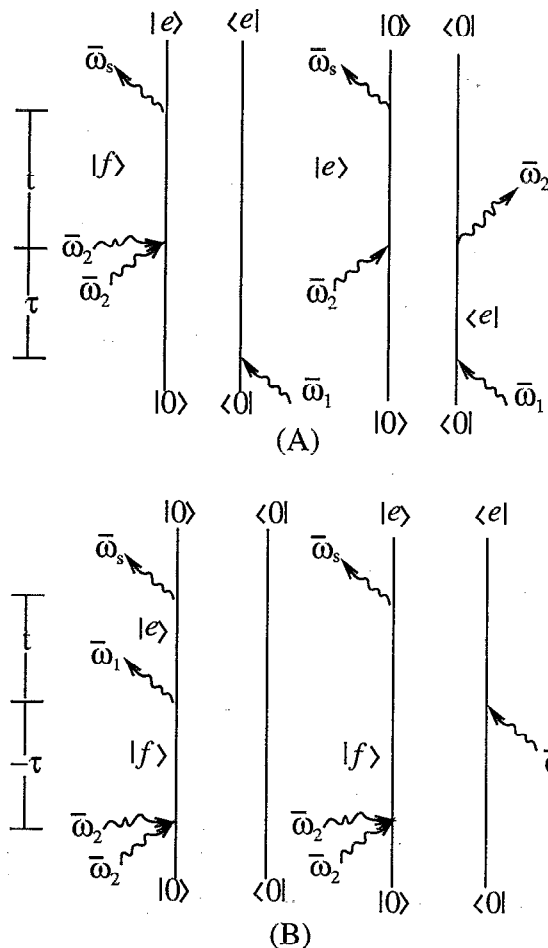


FIG. 7. Double-sided Feynman diagrams representing time domain four wave mixing for impulsive excitation and in the rotating-wave approximation. The left and the right vertical lines represent the ket and the bra of the density matrix, respectively, and the time runs from bottom to top. (A) positive delay ($\tau > 0$). (B) Negative delay ($\tau < 0$). $|0\rangle$, $|e\rangle$, and $|f\rangle$ denote ground state, single exciton states, and two exciton states (Fig. 5). Note that in (A), the right diagram is zero for a monolayer due to the momentum selection rule.

Then the exciton decays radiatively with rate $2\Gamma_1$. After a delay time τ , the sample interacts twice with E_2^{ext} and generates the signal. Therefore, the signal is proportional to $e^{-2\Gamma_1 \tau}$. Note that the right diagram of Fig. 7(A) contains a factor

$$|\mathbf{k}_2\rangle\langle\mathbf{k}_1| B_{\mathbf{k}_2}^+.$$

This is the usual contribution to the photon echo. However, here it vanishes for $\mathbf{k}_1 \neq \mathbf{k}_2$.

We next analyze the temporal profile of the signal. Equation (72) shows that the signal does not depend on the delay time τ , although its magnitude decreases exponentially. The temporal profile of the signal $P_{\mathbf{k}_s}(t, \tau \rightarrow +0)$ reflects the evolution of the density matrix element $|\mathbf{k}_2\mathbf{k}_2\rangle\langle\mathbf{k}_1|$, where

$$|\mathbf{k}_2\mathbf{k}_2\rangle = B_{\mathbf{k}_2}^+ B_{\mathbf{k}_2}^+ |0\rangle. \quad (75)$$

In the absence of radiative damping, the signal is proportional to the probability of the two exciton state $|\mathbf{k}_2\mathbf{k}_2\rangle$ to

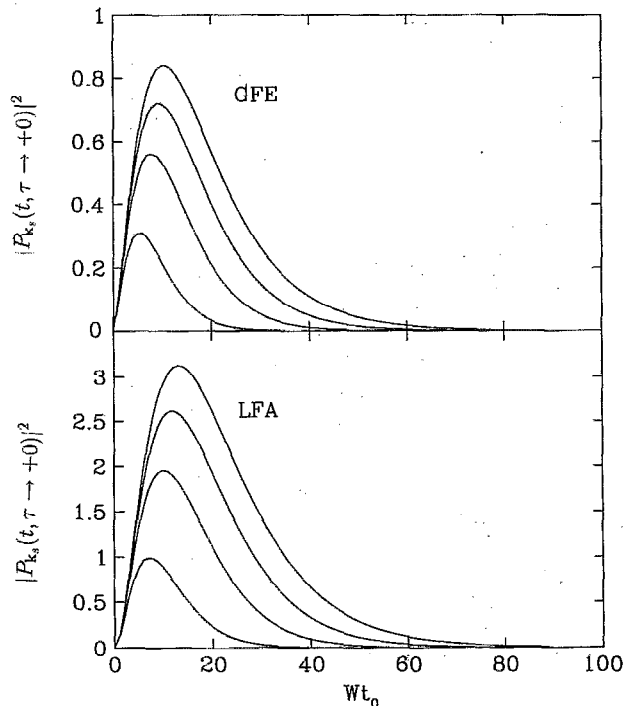


FIG. 8. The FWM signal $|P_{k_s}(t, \tau \rightarrow +0)|^2$ [Eq. (69)] vs time t for $k_2=0.4k_0\hat{y}$ and various values of k_1 along x direction. From top to bottom $k_1/k_0=0, 0.2\hat{x}, 0.4\hat{x}, 0.55\hat{x}$. Upper panel is the result of GFE. Lower panel is the result of LFA. The vertical line shows the relative magnitude of the signal. The rise time reflect exciton-exciton scattering, and the decay is radiative.

be scattered into $|k_1k_s\rangle \equiv B_{k_1}^+ B_{k_s}^+ |0\rangle$, where $k_s \equiv 2k_2 - k_1$. To get a rough estimate of the scattering time, consider the LFA Eq. (70) and set $\Gamma_i=0, i=1,2,s$. We see that the signal can show an oscillatory dependence on time. Starting at $t=0$, the signal increases and reaches its maximum at $T = \pi / (J_1 + J_s - 2J_2) \approx \pi (k_2 - k_1)^{-2} \mu^{-2}$. The rise time T is the scattering time from the state $|k_2k_2\rangle$ to $|k_1k_s\rangle$. In the presence of radiative damping, the radiative lifetime $\Gamma_k^{-1} \approx a^2 \mu^{-2} k_0^{-1}$ [see Eq. (25)] is much shorter than T , the two exciton state decays before it is fully scattered. $|P_{k_s}(t, \tau \rightarrow +0)|^2$ for $k_2=0.4k_0\hat{y}$ and various values of k_1 (along x direction) are shown in Fig. 8. The signal increases initially due to scattering and then decays radiatively.

From Fig. 8 we see that the peak of the signal decreases as k_1 increases and it eventually vanishes. The reason is as follow: as k_1 increases, $k_s = \sqrt{4k_2^2 + k_1^2}$ increases and finally when $|k_s|$ approach k_0 , $\Gamma(k_s) \rightarrow \infty$ [see Eq. (25)] and from Eq. (69) we see that $P_{k_s}^{(3)}(t, \tau) \rightarrow 0$. When $|k_s| > k_0$ the signal vanishes identically. Therefore, when $|2k_2 - k_1| > k_0$ a surface nonradiative [$\Gamma(k_s)=0$] exciton is created.

We next turn to negative delays $\tau < 0$. Figure 7(B) shows that the sample first interacts with E_2^{ext} twice creating a two exciton states $|k_2k_2\rangle$. Due to Pauli exclusion, the state $|k_2k_2\rangle$ is not an eigenstate. Then the two exciton state decays radiatively. After a delay time $-\tau$, the sample in-

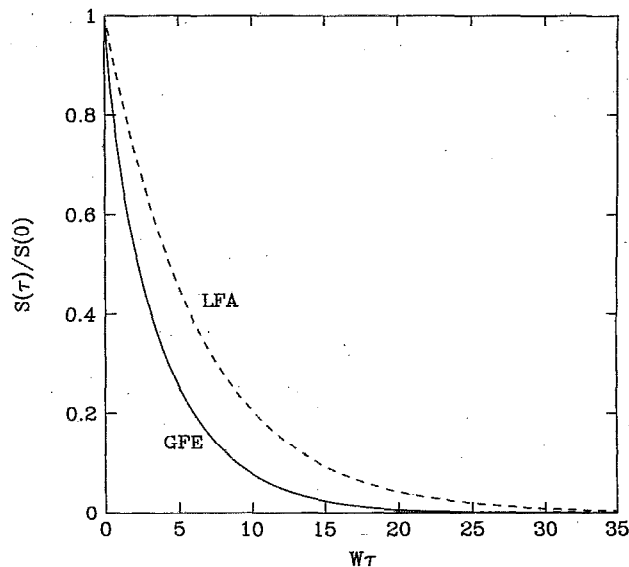


FIG. 9. Time integrated signal $S(\tau)$ [Eq. (71)] as a function of delay time $|\tau|$ for negative delays ($\tau < 0$). $k_1=0.5\hat{y}, k_2=0.3\hat{x}$. Solid line—GFE formulas; dashed line—the LFA.

teracts with E_1^{ext} once, resulting in the signal. The signal therefore starts at time $-\tau$. The time integrated signal $S(\tau)$ Eq. (71) representing the decay of two exciton states is displayed in Fig. 9. The dashed line is the result of the LFA, which gives $S(\tau) \sim \exp(-4\Gamma_2|\tau|)$, and decays slower than the solid line (GFE result). If $|k_2k_2\rangle$ were a two exciton eigenstate, then we expect

$$S(\tau) \sim e^{-\gamma^{(2)}(k_2)|\tau|}$$

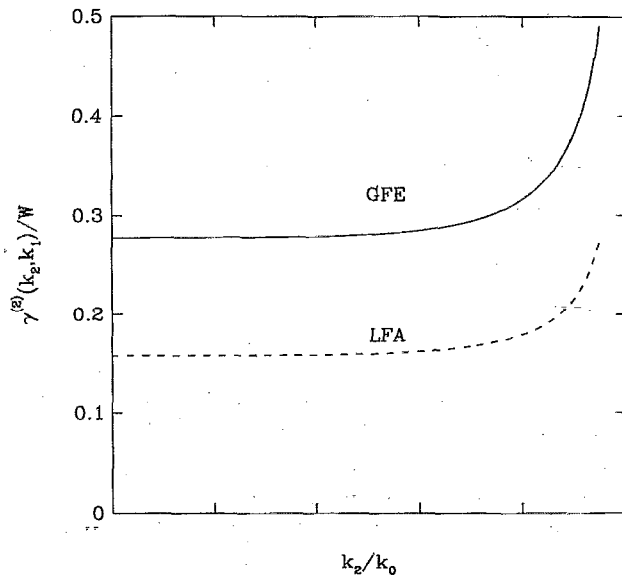


FIG. 10. The momentum dependent two exciton radiative decay rate probed by FWM $\gamma^{(2)}(k_2, k_1)$ as a function of k_2 (along x direction) for $k_1=0.9$ (along x direction). The solid (dash) line is the result of the GFE (LFA). The two curve has a constant ratio 1.76.

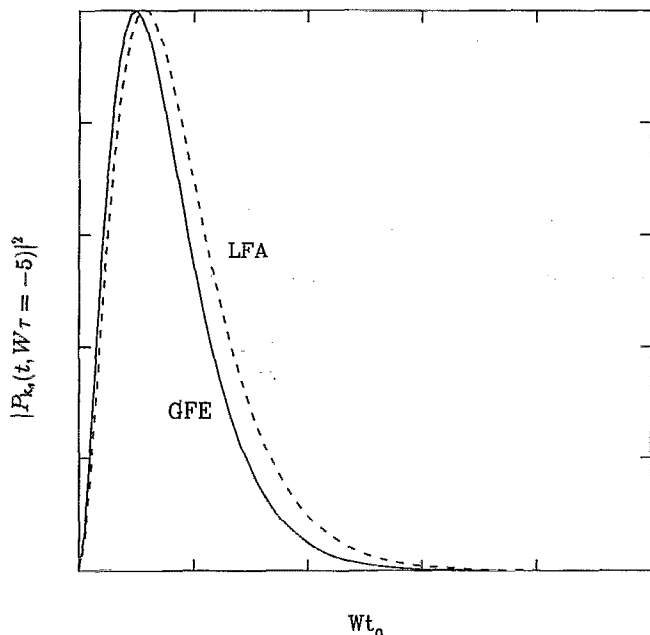


FIG. 11. The FWM signal intensity $|P_{k_s}(t, W\tau = -5)|^2$ Eq. (69) vs time $t_0 = t - |\tau|$. $k_1 = 0.5k_0\hat{x}$, $k_2 = 0.3k_0\hat{y}$. Solid line is the result of GFE. Dash line is the result of LFA, which was reduced by a factor of 6.6.

with decay rate $\gamma^{(2)}(k_2)$ which is independent on k_1 . However, since $|k_2k_2\rangle$ is not a two exciton eigenstate due to Pauli exclusion, the time dependent is nonexponential. We therefore define the average two exciton decay rate as

$$\gamma^{(2)}(k_2, k_1) \equiv \left[\int_0^\infty d|\tau| S(\tau)/s(0) \right]^{-1}. \quad (76)$$

Our numerical calculations show that the dependence of $\gamma^{(2)}(k_2, k_1)$ on k_1 is weak, which suggests that $|k_2k_2\rangle$ is close to a two exciton eigenstate. $\gamma^{(2)}(k_2, k_1)$ as a function of k_2 for $k_1 = 0.9$ (both k_2 and k_1 are along x direction) is shown in Fig. 10. In the LFA, $\gamma^{(2)}(k_2, k_1)$ is equal to the sum of the single exciton decay rates $4\Gamma(k_2)$ and is independent of k_1 , which implies that $|k_2k_2\rangle$ is a two exciton eigenstate. This is not the case for the GFE, where the two exciton decay is faster than the sum of single exciton decay rates. Their ratio is approximately a constant 1.76 (see Fig. 10).

Now we consider the temporal profile of the signal. Since it starts at time $|\tau|$, we define $t_0 = t - |\tau|$, and the LFA gives

$$|P_{k_s}^{(3)}(t_0, \tau)|^2 = e^{-4\Gamma_2|\tau|} |P_{k_s}^{(3)}(t_0, 0)|^2 \quad (77)$$

which implies that the temporal profile of the signal does not change with delay time τ , although its magnitude decreases exponentially. Numerical calculation of the GFE result Eq. (69) also shows that the temporal profile of the signal change very little with delay time τ for $\gamma^{(2)}(k_2, k_1)|\tau| < 2$ (i.e., $|\tau|$ is smaller than twice the two exciton radiative lifetime). Figure 11 shows the temporal

profile of the signal $|P_{k_s}^{(3)}(t_0, W\tau = 5.)|^2$. The LFA curve has a similar line shape as the GFE except that the magnitude is larger by a factor of 6.6.

VI. CONCLUSION

In this article we have demonstrated a resonant cooperativity of the nonlinear response for small aggregates. This cooperativity is lost when the size of aggregate is much larger than the optical wavelength. This suggests the existence of a coherence size of order of the optical wavelength within which the nonlinear optical response is cooperative. We found a new peak in the nonlinear reflection spectrum which cannot be accounted for by the LFA or a three level model. We showed that the new peak is caused by the sharp edge of two exciton density of states. However, this edge is not a sufficient condition for observing this additional peak. We have shown how the time resolved FWM signal from a molecular monolayer can be used to probe the momentum-dependent two exciton decay rates. We found that the two exciton decay rate is larger than the sum of the single exciton decay rates, while the LFA predicts them to be equal. The temporal profile of the impulsive FWM (for positive time delays) reveals information about the scattering and radiative decay of two exciton states. Since the radiative lifetime is much shorter than the scattering time, the two exciton state decays radiatively before it is fully scattered. When $|2k_2 - k_1| > k_0$, a nonradiative surface exciton is created.

Our numerical calculations also show that neglecting the radiative damping in the two exciton scattering matrix $\bar{\Gamma}$ is a good approximation. The reason is that the exciton created has an energy width of $\Gamma(k=0)$, which is much larger than the energy bandwidth of radiative excitons $J(k=\Omega/c) - J(k=0)$. Neglecting the radiative damping in $\bar{\Gamma}$ does not imply that we neglect effects of two exciton radiative decay. It simply assumes that the two particle states are polariton pairs which scatter as ordinary excitons. The radiative decay of two exciton states is incorporated in the single particle Green function G .

We have considered in this paper a two dimensional lattice. The application to a one dimensional lattice is straightforward. In that case, the projection of the wave vector on the lattice line is conserved, and k_i , $i=1,2,3,s$ in Eq. (33) should denote the projection of k_i , $i=1,2,3,s$ on the lattice line (rather than the plane).

Finally, the commonly used time domain response function $\hat{R}_{nm_1m_2m_3}(t_3, t_2, t_1)$ defined as²⁹

$$\begin{aligned} P_n^{(3)}(t) &= \int_0^\infty dt_1 \int_0^\infty dt_2 \int_0^\infty dt_3 \hat{R}_{nm_1m_2m_3}(t_3, t_2, t_1) \\ &\times E_{m_1}^{\text{ext}}(t-t_1-t_2-t_3) E_{m_2}^{\text{ext}}(t-t_2-t_3) \\ &\times E_{m_3}^{\text{ext}}(t-t_3), \end{aligned} \quad (78)$$

is related to the frequency domain response function [Eq. (15)] by

$$\begin{aligned} \hat{R}_{nm_1m_2m_3}(t_3, t_2, t_1) &= -\frac{1}{16\pi^3} \int d\omega_1 \int d\omega_2 \int d\omega_3 \\ &\times e^{-i\omega_1(t_1+t_2+t_3)} e^{-i\omega_2(t_2+t_3)} e^{-i\omega_3 t_3} \\ &\times \sum_p \hat{R}_{nm_1m_2m_3}(\omega_s; \omega_1, \omega_2, \omega_3), \end{aligned} \quad (79)$$

where $\omega_s = \omega_1 + \omega_2 + \omega_3$ and Σ_p denotes the sum over the six permutations of $m_1\omega_1, m_2\omega_2, m_3\omega_3$. The time domain response function may be useful in a variety of applications to ultrafast measurements.

ACKNOWLEDGMENTS

The support of the National Science Foundation, the Air Force Office of Scientific Research and the Center for Photoinduced Charge Transfer is gratefully acknowledged.

APPENDIX A: THE IMAGINARY PART OF THE MATERIAL SELF-ENERGY

In this Appendix, we evaluate $\text{Im } \phi$ in the dipole approximation for the geometry specified in Sec. III. Substituting Eq. (14) into Eq. (13), we have

$$\begin{aligned} \phi_{mn} &= \frac{1}{2\pi^2} \int d^3q \rho(-\mathbf{q}) \rho(\mathbf{q}) \frac{\omega^2}{\omega^2 - q^2 c^2 + i\eta} \\ &\times [\mu^2 - (\boldsymbol{\mu} \cdot \mathbf{q})^2 / q^2] e^{i\mathbf{q} \cdot \mathbf{R}_{mn}}. \end{aligned} \quad (A1)$$

The two dimensional spatial Fourier transform of ϕ_{mn} is

$$\text{Im } \phi(\mathbf{k}, \omega) = -\frac{2\pi}{a^2} \sum_{\mathbf{b}} \frac{(\omega/c)^2 \mu^2 - [\boldsymbol{\mu}^{\parallel} \cdot (\mathbf{k} + \mathbf{b})]^2 - (\mu^{\perp})^2 [(\omega/c)^2 - (\mathbf{k} + \mathbf{b})^2]}{\sqrt{(\omega/c)^2 - (\mathbf{k} + \mathbf{b})^2}} \Theta[(\omega/c)^2 - (\mathbf{k} + \mathbf{b})^2]. \quad (A5)$$

When ω is on resonant, and $(\omega/c)a \ll 1$, only the $\mathbf{b}=0$ term survives in this equation. Making the Markov approximation ($\omega = \Omega$), we obtain Eq. (25).

APPENDIX B: TWO EXCITON DENSITY OF STATES

In this Appendix, we derive an expression for the two exciton density of states with the center of mass momentum \mathbf{k} . Since the system includes the material and the quantum electromagnetic field, its eigenstates are mixtures of excitons and photons (polaritons). The exact definition of the density of states is as follows. Let P be a projection operator projecting the space of states of the joint system onto the subspace of two exciton states with the center of mass momentum \mathbf{k} and with no photons. Then the density of states $\rho_2(\mathbf{k}, \omega)$ is

$$\begin{aligned} \phi(\mathbf{k}, \omega) &= \sum_{\mathbf{R}_{mn}} \phi_{mn} e^{-i\mathbf{k} \cdot \mathbf{R}_{mn}} \\ &= \frac{1}{2\pi^2} \int d^3q \rho(-\mathbf{q}) \rho(\mathbf{q}) \frac{\omega^2}{\omega^2 - q^2 c^2 + i\eta} \\ &\times [\mu^2 - (\boldsymbol{\mu} \cdot \mathbf{q})^2 / q^2] \cdot M \sum_{\mathbf{b}} \delta_{\mathbf{q}^{\parallel}, \mathbf{k} + \mathbf{b}}. \end{aligned} \quad (A2)$$

Here \mathbf{k} is a two dimensional momentum vector in the first Brillouin zone, $\Sigma_{\mathbf{b}}$ denotes summation over reciprocal lattice, \mathbf{q}^{\parallel} and \mathbf{q}^{\perp} is the projection of \mathbf{q} in the plane and normal to the plane. For an infinite lattice, $M \delta_{\mathbf{q}^{\parallel}, \mathbf{k} + \mathbf{b}} \rightarrow (2\pi/a)^2 \delta(\mathbf{q}^{\parallel} - \mathbf{k} - \mathbf{b})$. Then we have

$$\begin{aligned} \phi(\mathbf{k}, \omega) &= \frac{2}{a^2} \sum_{\mathbf{b}} \int d\mathbf{q}^{\perp} \rho(-\mathbf{k} - \mathbf{b} - \mathbf{q}^{\perp}) \rho(\mathbf{k} + \mathbf{b} + \mathbf{q}^{\perp}) \\ &\times \frac{\omega^2 / c^2}{\omega^2 / c^2 - (q^{\perp})^2 - (\mathbf{k} + \mathbf{b})^2 + i\eta} \\ &\times \left\{ \mu^2 - \frac{[\boldsymbol{\mu}^{\parallel} \cdot (\mathbf{k} + \mathbf{b}) + \boldsymbol{\mu}^{\perp} \cdot \mathbf{q}^{\perp}]^2}{(q^{\perp})^2 + (\mathbf{k} + \mathbf{b})^2} \right\}. \end{aligned} \quad (A3)$$

Hereafter we will use the point dipole approximation, i.e., $\rho(\mathbf{q}) = 1$. We further use the identity

$$\begin{aligned} &\frac{1}{(\omega/c)^2 - (q^{\perp})^2 - (\mathbf{k} + \mathbf{b})^2 + i\eta} \\ &= \text{PP} \frac{1}{(\omega/c)^2 - (q^{\perp})^2 - (\mathbf{k} + \mathbf{b})^2} \\ &\quad - i\pi \delta[(\omega/c)^2 - (q^{\perp})^2 - (\mathbf{k} + \mathbf{b})^2]. \end{aligned} \quad (A4)$$

Here PP denote the principal part which contribute to the real part of $\phi(\mathbf{k}, \omega)$. The delta function in the above identity contributes to the imaginary part of $\phi(\mathbf{k}, \omega)$. Therefore,

$$\rho_2(\mathbf{k}, \omega) = -\frac{1}{\pi} \text{Im Tr}[P(\omega - H + i\eta)^{-1}P], \quad (B1)$$

where \hat{H} is the Hamiltonian of the joint system, and

$$\int_{-\infty}^{+\infty} d\omega \rho_2(\mathbf{k}, \omega) = N_2, \quad (B2)$$

where N_2 is the number of two exciton states with the center of mass momentum \mathbf{k} .

To evaluate the density of states $\rho_2(\mathbf{k}, \omega)$, we consider the model of interacting bosons with the Hamiltonian

$$\hat{H}_{\text{mat}} = \Omega \sum_n \hat{C}_n^+ \hat{C}_n + \sum_{m \neq n} J_{mn} \hat{C}_m^+ \hat{C}_n + \frac{g}{2} \sum_n (\hat{C}_n^+)^2 \hat{C}_n^2 \quad (B3)$$

with the Bose commutation relations

$$[\hat{C}_m^-, \hat{C}_n^+] = \delta_{mn}, \quad (\text{B4})$$

and the polarization

$$\hat{P}(\mathbf{r}) = \sum_m \hat{P}_m \rho_m(\mathbf{r} - \mathbf{R}_m), \quad \hat{P}_m(\mathbf{r}) = |\mu| (\hat{C}_m^- + \hat{C}_m^+), \quad (\text{B5})$$

with

$$\left| \int d\mathbf{r} \rho(\mathbf{r}) \right| = 1. \quad (\text{B6})$$

We get the expression for the density of states $\rho_g(\mathbf{k}, \omega)$ for this model with

$$\int_{-\infty}^{+\infty} d\omega \rho_g(\mathbf{k}, \omega) = N. \quad (\text{B7})$$

Taking the $g \rightarrow \infty$ limit of $\rho_g(\mathbf{k}, \omega)$, we obtain $\rho_2(\mathbf{k}, \omega)$. Note that due to the Pauli exclusion of excitons, the following relation holds

$$N_2 = N - 1. \quad (\text{B8})$$

We can see from Eqs. (B2)–(B8) that we have to be careful with the $g \rightarrow \infty$ limit, since

$$\lim_{g \rightarrow \infty} \int_{-\infty}^{+\infty} d\omega \rho_g(\mathbf{k}, \omega) \neq \int_{-\infty}^{+\infty} d\omega \lim_{g \rightarrow \infty} \rho_g(\mathbf{k}, \omega). \quad (\text{B9})$$

We begin by introducing a basis set in the relevant subspace $|\mathbf{p}\rangle$ by

$$|\mathbf{p}\rangle = C_p^+ C_{\mathbf{k}-\mathbf{p}}^+ |\Omega\rangle, \quad (\text{B10})$$

where $|\Omega\rangle$ is the vacuum state with no bosons and photons, and the operators C_p are of the form

$$C_p = \frac{1}{\sqrt{N}} \sum_n e^{-i\mathbf{p} \cdot \mathbf{R}_n} C_n. \quad (\text{B11})$$

The summation in Eq. (B11) is over all lattice sites. Making use of Eq. (B10) we can recast Eq. (B1) for $\rho_g(\mathbf{k}, \omega)$ in the form of a retarded Green function

$$\begin{aligned} \rho_g(\mathbf{k}, \omega) &= \frac{1}{\pi} \text{Im} \int_{-\infty}^{+\infty} dt e^{i\omega t} \\ &\times \sum_p \langle i [C_p(t) C_{\mathbf{k}-\mathbf{p}}(t), C_p^+(0) C_{\mathbf{k}-\mathbf{p}}^+(0)] \rangle. \end{aligned} \quad (\text{B12})$$

Evaluating the correlation function in the right-hand side of Eq. (B12) using the technique of Ref. 12, we obtain

$$\begin{aligned} \rho_g(\mathbf{k}, \omega) &= -\frac{1}{\pi} \text{Im} \left[\sum_p \frac{1}{\omega - \epsilon_{\mathbf{k},\mathbf{p}} + i\Gamma_{\mathbf{k},\mathbf{p}}} \right. \\ &+ gN^{-1} \sum_p \frac{1}{(\omega - \epsilon_{\mathbf{k},\mathbf{p}} + i\Gamma_{\mathbf{k},\mathbf{p}})^2} \\ &\times \left. \left(1 - gN^{-1} \sum_p \frac{1}{\omega - \epsilon_{\mathbf{k},\mathbf{p}} + i\Gamma_{\mathbf{k},\mathbf{p}}} \right)^{-1} \right], \end{aligned} \quad (\text{B13})$$

where

$$\epsilon_{\mathbf{k},\mathbf{p}} = 2\Omega + J(\mathbf{p}) + J(\mathbf{k} - \mathbf{p}), \quad (\text{B14})$$

$$\Gamma_{\mathbf{k},\mathbf{p}} = \Gamma(\mathbf{p}) + \Gamma(\mathbf{k} - \mathbf{p}). \quad (\text{B15})$$

Using the notation

$$F(\mathbf{k}, \omega) = \frac{1}{N} \sum_p \frac{1}{\omega - \epsilon_{\mathbf{k},\mathbf{p}} + i\Gamma_{\mathbf{k},\mathbf{p}}} \quad (\text{B16})$$

we can represent Eq. (B13) in the form

$$\begin{aligned} \rho_g(\mathbf{k}, \omega) &= -\frac{1}{\pi} \text{Im} \left[NF(\mathbf{k}, \omega) - \frac{g}{1 - gF(\mathbf{k}, \omega)} \cdot \frac{dF(\mathbf{k}, \omega)}{d\omega} \right]. \end{aligned} \quad (\text{B17})$$

Taking the $g \rightarrow \infty$ limit, we obtain from Eq. (B17)

$$\rho_2(\mathbf{k}, \omega) = -\frac{1}{\pi} \text{Im} \left[NF(\mathbf{k}, \omega) + \frac{d}{d\omega} \ln [F(\mathbf{k}, \omega)] \right]. \quad (\text{B18})$$

The first term in Eq. (B17) [or Eq. (B18)] is the density of states for noninteracting Bosons, and the second term is a correction due to interaction, which vanishes in the thermodynamical $N \rightarrow \infty$ limit. We finally get

$$\rho_2(\mathbf{k}, \omega) = -\frac{N}{\pi} \text{Im} [F(\mathbf{k}, \omega)]. \quad (\text{B19})$$

The normalized two exciton density of states is then given by Eq. (43). Performing the integration over ω in Eq. (B17) and Eq. (B18) and taking into account Eq. (B16), results in Eq. (B7) and Eq. (B8). The $g \rightarrow \infty$ limit and the integration over ω do not commute [Eq. (B9)]. The reason is that if we first integrate over ω , we take into account the pole in the second term of Eq. (B17) at $\omega \simeq g$ (for large g). But if we first set $g \rightarrow \infty$, the pole goes to infinity and does not contribute.

APPENDIX C: THE KRAMERS-KRONIG REPRESENTATION OF $\hat{\chi}^{(3)}$

In this Appendix we derive an expression for the nonlinear response function $\hat{\chi}^{(3)}$ in terms of an integral over energies of intermediate states [Eqs. (61) and (C15)]. For simplicity we take the incident beams to be perpendicular to the monolayer (homogeneous excitation). In this case we can start with the standard sum over states formula for the nonlinear response (see, e.g., Ref. 28)

$$\begin{aligned} \hat{\chi}^{(3)}(\omega_s; \omega_1, \omega_2, \omega_3) &= \sum_p \sum_{a,b,c} P_{0a} P_{ac} P_{cb} P_{b0} \cdot \left[\frac{1}{\omega_1 - \epsilon_b + i\eta} \frac{1}{\omega_1 + \omega_2 - \epsilon_c + i\eta} \right. \\ &\times \left. \left(\frac{1}{\omega_s - \epsilon_a + i\eta} + \frac{1}{-\omega_3 - \epsilon_a - i\eta} \right) + c'.c' \right]. \end{aligned} \quad (\text{C1})$$

Here $0, a, b, c$ stand for eigenstates (0 denotes the ground state) of the joint material + field system, P_{ij} are the matrix elements of the polarization operator \hat{P} . We work at zero temperature. Note that the summation in Eq. (C1) is over the eigenstates of the material system only,²⁸ therefore this

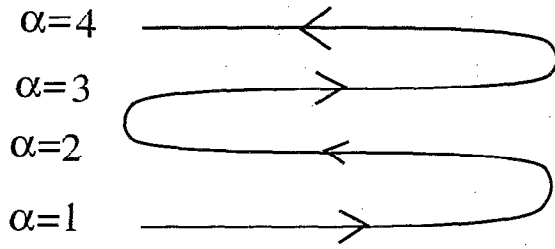


FIG. 12. Fourfold time loop for calculation of the correlation function in Eqs. (C6) and (C8), α denotes the component of the loop.

formula gives the nonlinear susceptibility $\hat{\chi}^{(3)}$ when the electromagnetic field treated classically. c', c'' denotes sending $\omega_i \rightarrow -\omega_i$, $i=1,2,3,s$ and then taking a complex conjugate. Introducing the quantity $\kappa(\epsilon', \epsilon, \epsilon'')$ [see Eq. (62)]

$$\kappa(\epsilon', \epsilon, \epsilon'') = (2\pi)^3 \sum_{a,b,c} P_{0a} P_{ac} P_{cb} P_{b0} \delta(\epsilon' - \epsilon_b) \times \delta(\epsilon - \epsilon_c) \delta(\epsilon'' - \epsilon_a), \quad (C2)$$

we can recast Eq. (C1) in the form Eq. (61) with $\kappa(\epsilon', \epsilon, \epsilon'')$ from Eq. (C2). To evaluate Eq. (C2) using Green functions, we present Eq. (C2) in the form

$$\kappa(\epsilon', \epsilon, \epsilon'') = \int_{-\infty}^{+\infty} \int_{-\infty}^{+\infty} \int_{-\infty}^{+\infty} d\tau_1 d\tau_2 d\tau_3 \times \langle 0 | \hat{P}(\tau_1 + \tau_2 + \tau_3) \hat{P}(\tau_1 + \tau_2) \hat{P}(\tau_1) \hat{P}(0) | 0 \rangle \times \exp(i\epsilon' \tau_1 + i\epsilon \tau_2 + i\epsilon'' \tau_3). \quad (C3)$$

Here $\hat{P}(\tau)$ is the polarization operator in the Heisenberg picture. In our case

$$\hat{P}(0) = \hat{P} = \mu \sum_n (B_n + B_n^\dagger) \quad (C4)$$

or for the boson model [see Eq. (B3)] it is given by

$$\hat{P} = \mu \sum_n (C_n + C_n^\dagger). \quad (C5)$$

We will perform the calculation for the boson model taking the limit $g \rightarrow \infty$ in the end. Introducing the four point correlation function $G(\omega_1, \omega_2, \omega_3, \omega_4)$ in the frequency domain

$$\langle 0 | \hat{P}(t_4) \hat{P}(t_3) \hat{P}(t_2) \hat{P}(t_1) | 0 \rangle = \int \frac{d\omega_1}{2\pi} \dots \int \frac{d\omega_4}{2\pi} 2\pi \delta(\omega_1 + \omega_2 - \omega_3 - \omega_4) \times \exp(-i\omega_4 t_4 - i\omega_3 t_3 + i\omega_2 t_2 + i\omega_1 t_1) \times G(\omega_1, \omega_2, \omega_3, \omega_4), \quad (C6)$$

we obtain from Eq. (C3)

$$\kappa(\epsilon', \epsilon, \epsilon'') = G(\epsilon', \epsilon - \epsilon', \epsilon - \epsilon'', \epsilon''). \quad (C7)$$

To evaluate the correlation function in Eq. (C6) we will use its path integral representation. To that end we introduce a time loop consisting of four time axis as it is shown in Fig. 12 (note that the Keldysh time loop consists

of two time axis). That means that for each variable O we introduce a set of variable $O^{(\alpha)}$, $\alpha=1,2,3,4$: $\alpha=1,3$ correspond to time varying from $-\infty$ to $+\infty$, and $\alpha=2,4$ to time varying from $+\infty$ to $-\infty$. The path integral representation of Eq. (C6) has the form

$$\langle 0 | \hat{P}(t_4) \hat{P}(t_3) \hat{P}(t_2) \hat{P}(t_1) | 0 \rangle = \langle \hat{P}^{(4)}(t_4) \hat{P}^{(3)}(t_3) \hat{P}^{(2)}(t_2) \hat{P}^{(1)}(t_1) \rangle_{\hat{S}}. \quad (C8)$$

The expectation value on the right-hand side of Eq. (C8) is taken with respect to the action

$$\hat{S} = \sum_{\alpha=1}^4 (-1)^{\alpha+1} S^{(\alpha)}, \quad S^{(\alpha)} = S[A^{(\alpha)}, C^{(\alpha)}, \bar{C}^{(\alpha)}], \quad (C9)$$

where $S[A, C, \bar{C}]$ is the action of the material system of interacting bosons described in Appendix B [Eq. (B3)–(B6)] coupled to the transverse electromagnetic field (see Ref. 12). The path integral is over the variables $A^{(\alpha)}, C^{(\alpha)}, \bar{C}^{(\alpha)}$; $\alpha=1,2,3,4$. $P^{(\alpha)}(t)$ has the form

$$P^{(\alpha)}(t) = \mu \sum_n [C_n^{(\alpha)}(t) + \bar{C}_n^{(\alpha)}(t)]. \quad (C10)$$

Switching to the effective action in the same manner as was done in Ref. 12 for the Keldysh time loop, we can recast Eq. (C8) in the form

$$\langle 0 | \hat{P}(t_4) \hat{P}(t_3) \hat{P}(t_2) \hat{P}(t_1) | 0 \rangle = \left\langle \hat{P}^{(4)}(t_4) \hat{P}^{(3)}(t_3) \hat{P}^{(2)}(t_2) \hat{P}^{(1)}(t_1) \times \exp \left[\frac{ig}{2} \sum_{\alpha=1}^4 \sum_n \int_{-\infty}^{+\infty} dt (-1)^\alpha \times \bar{C}_n^{(\alpha)} \bar{C}_n^{(\alpha)} C_n^{(\alpha)} C_n^{(\alpha)} \right] \right\rangle_{S_{\text{eff}}^{(0)}}, \quad (C11)$$

where $S_{\text{eff}}^{(0)}$ is the quadratic part of the effective action. The two point correlation functions with respect to $S_{\text{eff}}^{(0)}$ in the RWA have the form

$$-i \langle C_m^{(\alpha)}(t'') \bar{C}_n^{(\beta)}(t') \rangle = \int \frac{d\omega}{2\pi} \frac{d^2k}{(2\pi)^2} \exp[-i\omega(t'' - t')] + i\mathbf{k} \cdot (\mathbf{R}_m - \mathbf{R}_n) \hat{G}_{\alpha\beta}(\mathbf{k}, \omega), \quad (C12)$$

$$\hat{G}_{\alpha\beta}(\mathbf{k}, \omega) = 0 \quad \text{for } \alpha < \beta,$$

$$\hat{G}_{\alpha\beta}(\mathbf{k}, \omega) = \frac{1}{\omega - \Omega - J(\mathbf{k}) + i\Gamma(\mathbf{k})}$$

$$= \frac{1}{\omega - \Omega - J(\mathbf{k}) - i\Gamma(\mathbf{k})} \quad \text{for } \alpha > \beta,$$

$$\hat{G}_{\alpha\alpha}(\mathbf{k}, \omega) = \frac{1}{\omega - \Omega - J(\mathbf{k}) + i\Gamma(\mathbf{k})} \quad \text{for } \alpha=1,3,$$

$$\hat{G}_{\alpha\alpha}(\mathbf{k}, \omega) = -\frac{1}{\omega - \Omega - J(\mathbf{k}) - i\Gamma(\mathbf{k})} \quad \text{for } \alpha=2,4. \quad (C13)$$

Here and below we write $\langle \dots \rangle$ instead of $\langle \dots \rangle_{S_{\text{eff}}^{(0)}}$.

Expanding the exponent in Eq. (C11), and using the Wick theorem and some analytical properties of the Green functions in Eq. (C12), we obtain

$$\begin{aligned}
& \langle 0 | \hat{P}(t_4) \hat{P}(t_3) \hat{P}(t_2) \hat{P}(t_1) | 0 \rangle \\
&= \mu^4 \sum_{m_1, m_2, m_3, m_4} \left[\langle C_{m_2}^{(2)}(t_2) \bar{C}_{m_1}^{(1)}(t_1) \rangle \langle C_{m_4}^{(4)}(t_4) \bar{C}_{m_3}^{(3)}(t_3) \rangle + \langle C_{m_3}^{(3)}(t_3) \bar{C}_{m_2}^{(2)}(t_2) \rangle \right. \\
&\quad \times \langle C_{m_4}^{(4)}(t_4) \bar{C}_{m_1}^{(1)}(t_1) \rangle + \langle C_{m_3}^{(3)}(t_3) \bar{C}_{m_1}^{(1)}(t_1) \rangle \langle C_{m_4}^{(4)}(t_4) \bar{C}_{m_2}^{(2)}(t_2) \rangle \\
&\quad + \sum_{N=1}^{\infty} 2(ig)^N \int d\tau_1 \cdots d\tau_N \sum_{n_1 \cdots n_N} \langle C_{n_1}^{(2)}(\tau_1) \bar{C}_{m_1}^{(1)}(t_1) \rangle \langle C_{n_1}^{(1)}(\tau_1) \bar{C}_{m_2}^{(2)}(t_2) \rangle \\
&\quad \times \langle C_{n_2}^{(2)}(\tau_2) \bar{C}_{n_1}^{(2)}(\tau_1) \rangle^2 \cdots \langle C_{n_N}^{(2)}(\tau_N) \bar{C}_{n_{N-1}}^{(2)}(\tau_{N-1}) \rangle^2 \langle C_{m_3}^{(3)}(t_3) \bar{C}_{n_N}^{(2)}(\tau_N) \rangle \langle C_{m_4}^{(4)}(t_4) \bar{C}_{n_N}^{(2)}(\tau_N) \rangle \\
&\quad + \sum_{L=1}^{\infty} 2(-ig)^L \int d\tau'_1 \cdots d\tau'_L \sum_{e_1 \cdots e_L} \langle C_{e_1}^{(3)}(\tau'_1) \bar{C}_{m_1}^{(1)}(t_1) \rangle \langle C_{e_1}^{(3)}(\tau'_1) \bar{C}_{m_2}^{(2)}(t_2) \rangle \\
&\quad \times \langle C_{e_2}^{(3)}(\tau'_2) \bar{C}_{e_1}^{(3)}(\tau'_1) \rangle^2 \cdots \langle C_{e_L}^{(3)}(\tau'_L) \bar{C}_{e_{L-1}}^{(3)}(\tau'_{L-1}) \rangle \langle C_{m_4}^{(4)}(t_4) \bar{C}_{e_L}^{(3)}(\tau'_L) \rangle + \sum_{N,L=1}^{\infty} 2(ig)^N \\
&\quad \times (-ig)^L \int d\tau_1 \cdots d\tau_N \int d\tau'_1 \cdots d\tau'_L \sum_{n_1, \dots, n_N, e_1, \dots, e_L} \langle C_{n_1}^{(2)}(\tau_1) \bar{C}_{m_1}^{(1)}(t_1) \rangle \langle C_{n_1}^{(2)}(\tau_1) \bar{C}_{m_2}^{(2)}(t_2) \rangle \\
&\quad \times \langle C_{n_2}^{(2)}(\tau_2) \bar{C}_{n_1}^{(2)}(\tau_1) \rangle^2 \cdots \langle C_{n_N}^{(2)}(\tau_N) \bar{C}_{n_{N-1}}^{(2)}(\tau_{N-1}) \rangle^2 \langle C_{e_1}^{(3)}(\tau'_1) \bar{C}_{n_N}^{(2)}(\tau_N) \rangle^2 \\
&\quad \times \langle C_{e_2}^{(3)}(\tau'_2) \bar{C}_{e_1}^{(3)}(\tau'_1) \rangle^2 \cdots \langle C_{e_L}^{(3)}(\tau'_L) \bar{C}_{e_{L-1}}^{(3)}(\tau'_{L-1}) \rangle^2 \langle C_{m_4}^{(4)}(t_4) \bar{C}_{e_L}^{(3)}(\tau'_L) \rangle \langle C_{m_3}^{(3)}(t_3) \bar{C}_{e_L}^{(3)}(\tau'_L) \rangle \left. \right]. \quad (\text{C14})
\end{aligned}$$

Switching to the frequency and momentum domain, substituting the Green functions [Eq. (C12)] and making use of Eqs. (C6) and (C7), and taking the limit $g \rightarrow \infty$, we obtain

$$\kappa(\epsilon', \epsilon, \epsilon'') = \kappa_0(\epsilon', \epsilon, \epsilon'') + \kappa_{2f}(\epsilon', \epsilon, \epsilon'') + \kappa_{\text{int}}(\epsilon', \epsilon, \epsilon''), \quad (\text{C15a})$$

$$\kappa_0 = -\frac{16\pi\mu^4\Gamma_0^2}{(\epsilon' - E_0)^2 + \Gamma_0^2} \cdot \frac{1}{(\epsilon'' - E_0)^2 + \Gamma_0^2} \delta(\epsilon), \quad (\text{C15b})$$

$$\begin{aligned}
\kappa_{2f} &= -\frac{16\pi\mu^4\Gamma_0^2}{(\epsilon' - E_0)^2 + \Gamma_0^2} \cdot \frac{1}{(\epsilon'' - E_0)^2 + \Gamma_0^2} \\
&\quad \times \delta(\epsilon'' + \epsilon' - \epsilon) - \frac{16\pi\mu^4\Gamma_0^2}{(\epsilon' - E_0)^2 + \Gamma_0^2} \\
&\quad \cdot \frac{1}{(\epsilon - \epsilon' - E_0)^2 + \Gamma_0^2} \delta(\epsilon'' - \epsilon'), \quad (\text{C15c})
\end{aligned}$$

$$\begin{aligned}
\kappa_{\text{int}} &= -\frac{8\pi\mu^4\Gamma_0^2}{(\epsilon' - E_0)^2 + \Gamma_0^2} \\
&\quad \cdot \frac{1}{(\epsilon'' - E_0)^2 + \Gamma_0^2} \left[\frac{1}{\epsilon - \epsilon' - E_0 + i\Gamma_0} \right. \\
&\quad \cdot \frac{1}{\epsilon - \epsilon'' - E_0 + i\Gamma_0} \cdot \frac{1}{F(\epsilon)} + \text{c.c.} \left. \right], \quad (\text{C15d})
\end{aligned}$$

where $E_0 = \Omega + J(\mathbf{k}=0)$, $\Gamma_0 = \Gamma(\mathbf{k}=0)$ and $F(\epsilon) = F(\mathbf{k}=0, \epsilon)$. This formula was obtained starting with Eq. (C1), where the a, b, c summations run over $|0\rangle$, $\{|e\rangle\}$, and $\{|f\rangle\}$ (Fig. 5). κ_0 corresponds to the choice $a = \{|e\rangle\}$, $c = |0\rangle$, $b = \{|e\rangle\}$ and represents the nonlinear response of a two level system coupled to photons. κ_{2f} corresponds to process with $c = \{|f\rangle\}$ for the case of noninteracting excitons. Therefore, the contributions of κ_0 and κ_{2f} to $\hat{\chi}^{(3)}$ cancel since they give $\hat{\chi}^{(3)} = 0$ of free polaritons, and only the κ_{int} term contributes to $\hat{\chi}^{(3)}$.

¹F. F. So, S. R. Forrest, Y. Q. Shi, and W. H. Steier, Appl. Phys. Lett. **56**, 674 (1990); F. F. So and S. R. Forrest, Phys. Rev. Lett. **66**, 2649 (1991).

²M. Orrit, C. Aslangul, and Ph. Kottis, Phys. Rev. B **25**, 7263 (1982); M. Orrit and Ph. Kottis, Adv. Chem. Phys. **74**, 1 (1988).

³D. Mobius and H. Kuhn, Isr. J. Chem. **18**, 375 (1979); J. Appl. Phys. **64**, 5138 (1988).

⁴A. Laubereau (private communication).

- ⁵H. Fidler, J. Knoester, and D. A. Wiersma, *J. Chem. Phys.* **98**, 6564 (1993).
- ⁶J. Knoester and S. Mukamel, *Phys. Rep.* **205**, 1 (1991).
- ⁷F. C. Spano, J. R. Kuklinski, and S. Mukamel, *Phys. Rev. Lett.* **65**, 211 (1990); *J. Chem. Phys.* **94**, 7534 (1991); A. A. Muentner, D. V. Brumbaugh, J. Apolito, L. A. Horn, F. C. Spano, and S. Mukamel, *J. Phys. Chem.* **96**, 2783 (1992).
- ⁸F. C. Spano and S. Mukamel, *Phys. Rev. Lett.* **66**, 1197 (1991).
- ⁹S. Mukamel, in *Nonlinear Optical Properties of Organic Molecules and Crystals*, edited by J. Zyss (Academic, New York, 1993).
- ¹⁰Y. Ohfuti and K. Cho, in *Proceedings of the International Symposium on Science and Technology of Mesoscopic Structures*, Nara, Japan, 1991 (Springer, Berlin, to be published); *Jpn. J. Appl. Phys. Series 9*, 197 (1993).
- ¹¹J. K. Jenkins and S. Mukamel, *J. Chem. Phys.* **98**, 7046 (1993).
- ¹²V. Chernyak and S. Mukamel, *J. Chem. Phys.* (to be published); *Phys. Rev. B* **48**, 2470 (1993).
- ¹³N. Wang, A. A. Muentner, and S. Mukamel, *J. Chem. Phys.* **99**, 3604 (1993).
- ¹⁴See, *Excitons in Confined Systems*, edited by A. Andrea, R. Del Sole, and R. Girlanda (The Institute of Physics, Bristol, 1992).
- ¹⁵L. Schultheis, J. Kuhl, A. Honold, and C. W. Tu, *Phys. Rev. Lett.* **57**, 1635, 1797 (1986).
- ¹⁶J. L. Oudar, D. Hulin, A. Migus, A. Antonetti, and F. Alexandre, *Phys. Rev. Lett.* **55**, 2074 (1985).
- ¹⁷M. T. Portella, J.-Y. Bigot, R. W. Schoenlein, J. E. Cunningham, and C. V. Shank, *Appl. Phys. Lett.* **60**, 2123 (1992).
- ¹⁸B. Fluegel, N. Peyghambarian, G. Olbright, M. Lindberg, S. W. Koch, M. Joffre, D. Hulin, A. Migus, and A. Antonetti, *Phys. Rev. Lett.* **59**, 2588 (1987); *Phys. Rev. B* **38**, 7615 (1988).
- ¹⁹M. Lindberg and S. W. Koch, *Phys. Rev. B* **38**, 1631 (1988).
- ²⁰R. C. Miller, D. A. Kleinman, A. C. Gossard, and O. Manteanu, *Phys. Rev. B* **25**, 6545 (1982); Q. Fu, D. Lee, A. Mysyrowicz, A. V. Nurmikko, R. C. Gunshor, and L. A. Kolodziejewski, *ibid.* **37**, 8791 (1988).
- ²¹Y. Z. Hu, S. W. Koch, M. Lindberg, N. Peyghambarian, E. L. Pollock, and F. F. Abraham, *Phys. Rev. Lett.* **64**, 1805 (1990).
- ²²S. Weiss, M.-A. Mycek, J.-Y. Bigot, S. Schmitt-Rink, and D. S. Chemla, *Phys. Rev. Lett.* **69**, 2685 (1992); J.-Y. Bigot, M.-A. Mycek, S. Weiss, R. G. Ulbrich, and D. S. Chemla, *Phys. Rev. Lett.* **70**, 3307 (1993).
- ²³S. Schmitt-Rink, S. Mukamel, K. Leo, J. Shah, and D. S. Chemla, *Phys. Rev. A* **44**, 2124 (1991).
- ²⁴S. Mukamel, Z. Deng, and J. Grad, *J. Opt. Soc. Am. B* **5**, 804 (1988).
- ²⁵J. A. Leegwater and S. Mukamel, *Phys. Rev. A* **46**, 452 (1992).
- ²⁶J. Knoester, *Phys. Rev. Lett.* **68**, 655 (1992).
- ²⁷M. Cho, N. F. Scherer, G. R. Fleming, and S. Mukamel, *J. Chem. Phys.* **96**, 5618 (1992).
- ²⁸B. J. Orr and J. F. Ward, *Mol. Phys.* **20**, 513 (1971).
- ²⁹S. Mukamel and R. F. Loring, *J. Opt. Soc. Am. B* **3**, 595 (1986).